Biogeosciences Discuss., 12, 1975–2019, 2015
www.biogeosciences-discuss.net/12/1975/2015/
doi:10.5194/bgd-12-1975-2015
© Author(s) 2015. CC Attribution 3.0 License.

Biogeosciences Discussions
Open Access

This discussion paper is/has been under review for the journal Biogeosciences (BG).
Please refer to the corresponding final paper in BG if available.

Seasonal dynamics of organic carbon and metals in thermokarst lakes from the discontinuous permafrost zone of western Siberia

R. M. Manasypov[1], S. N. Vorobyev[1], S. V. Loiko[1], I. V. Kritzkov[1], L. S. Shirokova[2,3], V. P. Shevchenko[4], S. N. Kirpotin[1], S. P. Kulizhsky[1], L. G. Kolesnichenko[1], V. A. Zemtzov[1], V. V. Sinkinov[1], and O. S. Pokrovsky[1,2]

[1]Tomsk State University, 634050, Tomsk, 36 Lenin av., Russia
[2]Geosciences and Environnement Toulouse, UMR 5563 CNRS, Université de Toulouse, 14 avenue Edouard Belin, 31400, France
[3]Institute of Ecological Problems of the North UroRAS, 163061, Arkhangelsk, Nab. Severnoj Dviny, 23, Russia
[4]P.P. Shirshov Institute of Oceanology of the Russian Academy of Sciences, 36 Nakhimovsky Prospekt, 117997 Moscow, Russia

Received: 3 December 2014 – Accepted: 18 December 2014 – Published: 30 January 2015

Correspondence to: O. S. Pokrovsky (oleg@get.obs-mip.fr)

Published by Copernicus Publications on behalf of the European Geosciences Union.

Abstract

Western Siberia's thermokarst (thaw) lakes extend over a territory spanning over a million km^2; they are highly dynamic hydrochemical systems that receive chemical elements from the atmosphere and surrounding peat soil and vegetation, and exchange greenhouse gases with the atmosphere, delivering dissolved carbon and metals to adjacent hydrological systems. This work describes the chemical composition of ~ 130 thermokarst lakes of the size range from a few m^2 to several km^2, located in the discontinuous permafrost zone. Lakes were sampled during spring floods, just after the ice break (early June), the end of summer (August), the beginning of ice formation (October) and during the full freezing season in winter (February). Dissolved organic carbon (DOC) and the major and trace elements do not appreciably change their concentration with the lake size increase above 1000 m^2 during all seasons. On the annual scale, the majority of dissolved elements including organic carbon increase their concentration from 30 to 500 %, with a statistically significant ($p < 0.05$) trend from spring to winter. The maximal increase in trace element (TE) concentration occurred between spring and summer and autumn and winter. The ice formation in October included several stages: first, surface layer freezing followed by crack (fissure) formation with unfrozen water from the deeper layers spreading over the ice surface. This water was subsequently frozen and formed layered ice rich in organic matter. As a result, the DOC and metal concentrations were the highest at the beginning of the ice column and decreased from the surface to the depth. A number of elements demonstrated the accumulation, by more than a factor of 2, in the surface (0–20 cm) of the ice column relative to the rest of the ice core: Mn, Fe, Ni, Cu, Zn, As, Ba and Pb. The main consequences of discovered freeze-driven solute concentrations in thermokarst lake waters are enhanced colloidal coagulation and the removal of dissolved organic matter and associated insoluble metals from the water column to the sediments. The measured distribution coefficient of TE between amorphous organo-ferric coagulates and lake water (< 0.45 µm) were similar to those reported earlier for Fe-rich colloids

BGD
12, 1975–2019, 2015

and low molecular weight (< 1 kDa) fractions of thermokarst lake waters, suggesting massive co-precipitation of TE with amorphous Fe oxy(hydr)oxide stabilized by organic matter. Although the concentration of most elements is lowest in spring, this period of maximal water coverage of land creates a significant reservoir of DOC and soluble metals in the water column that can be easily mobilized to the hydrological network. The highest DOC concentration observed in the smallest (< 100 m^2) water bodies in spring suggests their strongly heterotrophic status and, therefore, elevated CO_2 flux from the lake surface to the atmosphere.

1 Introduction

Western Siberia's thermokarst (thaw) lakes extend over a territory spanning over a million km^2; they are highly dynamic hydrochemical systems that receive chemical elements from the atmosphere and surrounding peat soil and exchange greenhouse gases (GHG) with the atmosphere, delivering dissolved carbon and metals to adjacent hydrological systems. Because more permafrost will continue to thaw due to climate warming, which is heavily intensified in this region, the directions and magnitude of lake–river exchange processes may be significantly modified, seriously affecting the biogeochemical fluxes both on land and in the coastal zone of the Arctic Ocean.

In contrast to relatively good understanding of western Siberia thermokarst lake functioning during the active (summer) season (Walter et al., 2006, 2008; Walter Anthony et al., 2012; Audry et al., 2011; Pokrovsky et al., 2011, 2013, 2014; Shirokova et al., 2009, 2013; Karlsson et al., 2012, 2014; Manasypov et al., 2014), the intra-annual variations of lake water chemistry including glacial periods and spring floods remained, up to the present time, virtually unexplored. At the same time, the glacial season is extremely important in GHG regulation in boreal lakes, due to significant accumulation of gases under the ice and their liberation during the ice thaw (Karlsson et al., 2013). Similarly, the ice formation period provides important insights into the solute concentration and colloid coagulation mechanisms, given the main particularity

BGD
12, 1975–2019, 2015

of shallow thermokarst lakes in western Siberia – their full freezing during winter (Pokrovsky et al., 2011). The possibility of complete freezing of western Siberia thermokarst lakes contrasts with the majority of other thermokarst lakes studied all over the world, such as from the Kolyma low land (Walter Anthony et al., 2014), the Lena Delta (Boike et al., 2013), the Mackenzie Delta plain (Tank et al., 2009, 2011; Grosse et al., 2013; Walter Anthony and Anthony, 2013) and the north of Quebec (Laurion et al., 2010; Negandhi et al., 2013), which often have a depth of more than 2 m and as such do not freeze till the bottom, while exhibiting chemical and thermal stratification of the water column. Another important difference of thermokarst western Siberia lakes from other high-latitude lakes is the lack of a connection to the underground network in the former ones. Therefore, lake drainage to the hydrological network occurs only via surface flow (Kirpotin et al., 2008), without subsurface flow as in Alaska (Roach et al., 2011).

Towards filling the gap in our knowledge of seasonal variations of thermokarst lake chemical composition, we present in this work results of analysis of water and ice sampled in thermokarst lakes of various sizes, from several m to several km in diameter, during four main hydrological seasons, June, August, October and February. We aimed to address the following specific questions. (i) Is there a statistically significant difference in major and trace element concentrations between different seasons, with a broad range of the lake size? (ii) How significant is lake size and lake water residence time control for lake water chemical composition during different seasons? (iii) What are the mechanisms and degrees of element differentiation during ice formation and full water column freezing? (iv) How significant is water dilution during spring melt and what are the consequences for river water feeding by lakes during this period?

Answering these questions should provide the first insights into thermokarst lake biogeochemical functioning and help to constrain the impact of lake water metal and carbon cycling on river water composition and greenhouse gas exchange with the atmosphere in the course of a year. From a larger perspective, understanding seasonal patterns of dissolved organic carbon and metal micronutrients in these

BGD
12, 1975–2019, 2015

shallow but highly abundant water bodies, different from previously studied glacial and deep thermokarst/yedoma lakes, should allow predictions of phytoplankton activity, sedimentation and microbial respiration on the annual scale, necessary for evaluation of the net ecosystem exchange under various climate change scenarios.

2 Study site description and analytical and statistical methods

Our study site, which is located in the central part of western Siberia (63.5° N, 75.4° E, Nojabrsk administrative region), contains discontinuous permafrost within the northern taiga geographical sub-zone over Late Pleistocene sand and clay deposits that are covered by a layer of peat that is 1–2 m thick (Fig. S1 in the Supplement). All the lakes in this study were located at watershed divides between adjacent rivers. The water bodies ranged from a few m to several km in diameter and had a similar depth of 1.0±0.5 m under normal precipitation/evaporation conditions. The morphology, hydrology and water balance of thermokarst lakes were extensively studied during four field campaigns in June, August, and October 2013 and February 2014. The detailed depth mapping of ~ 20 large lakes was performed via echosounder from a rubber boat; the denivelation and the direction of the water flow were measured using a levelling network in several narrow profiles; the depth and density of snow were measured over a model site of 500 m × 500 m that included lakes, a palsa bog, some streams and an adjacent forested riparian zone. The water residence time was calculated from the annual precipitation and evapotranspiration measured at the neighboring meteostation of the Russian Hydrometeorological Station, the annual runoff of the territory and the water volume of the lakes.

Water samples were collected from the PVC or rubber boat for large lakes or directly from the lake center for small (< 50 m diameter) water bodies during June and August 2013 and from the ice during the October 2013 and February 2014 sampling campaigns. A list of sampled water bodies and their main hydrological and hydrochemical characteristics is presented in Table 1. The sampling and filtration

BGD
12, 1975–2019, 2015

methods used in this study, as well as the chemical analysis techniques, are identical to those utilized in our previous studies (Pokrovsky et al., 2011). An ultra-clean sampling procedure was used for all manipulations in the field (Shirokova et al., 2010). Water samples were filtered on-site through sterile single-use Minisart® filter units (Sartorius, acetate cellulose filters) with a pore size of 0.45 µm. For TE analysis, samples were acidified to pH = 2 with double-distilled HNO_3. Dissolved oxygen, pH, and Eh were measured on-site with uncertainties of 5 %, 0.02 units, and 2 mV, respectively, using a WTW® oximeter and a Hanna® portable pH meter with an Eh/pH electrode.

Major anion concentrations (Cl^- and SO_4^{2-}) were measured by ion chromatography (HPLC, Dionex ICS 2000) with an uncertainty of 2 %. DOC was analyzed using a carbon total analyzer (Shimadzu TOC 6000) with an uncertainty better than 3 %. Major and trace elements were determined with an ICP-MS Agilent ce 7500, routinely used in our laboratory for the analysis of samples from boreal organic-rich lakes (cf. Pokrovsky et al., 2013). Indium and rhenium were used as external standards. The SLRS-5 international geostandard (Riverine Water Reference Material for Trace Metals certified by the National Research Council of Canada) was used to check the accuracy and reproducibility of each analysis (Yeghicheyan et al., 2014). We obtained good agreement between replicate measurements of SLRS and certified values (relative difference less than 10 % SD for repeated measurements), except for B and P (30 %). In addition to TE analysis using the Agilent quadropole instrument, 60 % of samples were processed with an ultra-sensitive Element XR ICP-MS instrument operated in low- and medium-resolution mode. Using this ICP-MS greatly increased the detection limits of a number of elements and improved the precision of the analyses, while avoiding interferences. The uncertainty of the Element XR analysis was ≤ 5 %, while its detection limit was a factor of 100 lower than the traditional (Agilent) instrument. The average agreement between the two ICP-MS instruments for the majority of the TE was 10–15 %.

The ice of the lake water column was sampled in February 2014 from the central part of the lakes using titanium circular ice coring. The ice core was cut using a Ti saw in

BGD
12, 1975–2019, 2015

10 cm slices, melted at room temperature and filtered through 0.45 µm filters. The ice filtrate was processed in the same way as the lake water. In three instances, the bottom layer of unfrozen water below the ice column could be collected for analysis. Chemical composition of Fe-rich coagulates collected from the ice surface in early June was measured by ICP-MS after full dissolution of the solid using a microwave acid digestion procedure (Stepanova et al., 2014). Particulate organic carbon was quantified using a TOC_{CHS} instrument. The freeze-dried precipitates were characterized by scanning electron microscopy (SEM) using a Jeol JSM840a, and by X-ray diffraction using an INEL CPS 120 CoK_{α}.

The element concentrations were analyzed using best fit functions based on the least squares method, Pearson correlation and one-way ANOVA. Regressions and power functions were used to examine the relationships between the elemental concentrations and the lake surface areas. The ANOVA was carried out using Dunn's method because each zone utilized a different number of samples (SigmaPlot version 11.0/Systat Software, Inc).

3 Results

3.1 Effect of the lake size on dissolved carbon and related element concentrations in the water column

The lists of sampled water bodies with their main hydrophysical and hydrochemical characteristics and their geographical localization are given in Table 1 and Fig. 1, respectively. Within the range of 100 to 2×10^6 m^2 lake size, the effect of the lake size on major and trace element concentration is not strongly pronounced. The Spearman (R_S) rank correlation coefficient was below 0.5 for all elements over all seasons, suggesting a quite weak if not negligible impact of the lake size on lake water chemical composition.

BGD
12, 1975–2019, 2015

Only in spring, for the range of 0.1 to 2×10^6 m^2 lake size, was Pearson's coefficient statistically significant ($p < 0.05$), and suggested a decrease in the following element concentrations with the logarithm of the lake size increase: DOC (−0.69), V (−0.43), Cr (−0.54), Ni (−0.58), Cu (−0.63), Ga (−0.71), As (−0.53), Cd (−0.69), and Pb (−0.8). Such a semi-logarithmic negative relationship suggests a rapid decrease in the concentration within the small water bodies and its relative stability in large lakes. Indeed, this trend was mainly due to the increase in certain element concentrations in the smallest (< 10–100 m^2) water bodies rather than a steady evolution of concentrations in medium-size and large water bodies.

The DOC concentration exhibited two maxima, at 1000–10 000 m^2 surface area in summer and autumn and in micro-depressions (< 1 m^2) in spring (Fig. 2). The nature of the DOC was different among different seasons, because the slope of the UV_{280}–[DOC] dependence increased in the order spring (0.023) < summer (0.034) < autumn (0.046) < winter (0.063). The ratio of UV_{280} to [DOC] during four sampled seasons demonstrated the lowest values in spring and the highest in autumn–winter, being independent of the lake size (Fig. 3).

None of the seasons demonstrated a statistically significant dependence between the element concentration and the water body size above 100 m^2. There was quite high variability in the major element concentration in lakes of the same size range, typically over 2 orders of magnitude, as can be seen for Ca and Si in Fig. 4a and b, respectively. There was a general increase in the lake water pH with the increase in the lake size, detectable during all seasons (Fig. 5). The small-size lakes sampled in spring exhibited the lowest pH, between 3.5 and 4.5, whereas the larger lakes (> 1000 m^2) in summer demonstrated a pH of 5 to 6. Similar to major cations, the major anion concentration did not demonstrate any discernable trend with the lake surface area; only Cl^- yielded the minimal concentration for the lakes of ca. 100 m^2 surface area (Table S1 in the Supplement). Dissolved inorganic carbon (DIC) concentration was a factor of 30 lower than [DOC], without a statistically significant trend with the lake size (not shown). The illustration of the lake surface area effect on trace element concentrations during all

BGD
12, 1975–2019, 2015

four sampled seasons is given in Fig. S2 in the Supplement for Fe, Al, Mn, Zn, Cu, Pb, Mo, V, As, and Sb, and the primary data are listed in Table S1.

There was a limited degree of element correlation with either DOC or Fe considering all seasons of the year, as illustrated in Pearson pair correlation (Table S2). Examples of mostly pronounced correlations between Fe and DOC, As and Fe, and Cd and DOC are shown in Fig. 6. Considering all seasons simultaneously, several groups of elements could be distinguished based on this correlation analysis:

1. elements correlated with Fe ($R_{Fe} > R_{DOC}$): Cl, SO_4, Mg, Ca, Sr, Ba, Rb, Al, Ga, Cr, Mn, Co, Ni, Si, As, REEs and U.
2. elements correlated with DOC rather than with Fe ($R_{DOC} > R_{Fe}$): Cu, Zn, Cd and Pb.
3. elements strongly correlated with Al ($R > 0.6$ at $p < 0.05$): Be, Si, K, Rb, Cs, Sr, Ba, Ti, V, Cr, Co, Cu, Ga, As, Sb, REEs, W and U.
4. elements exhibiting high pair correlations ($R \geq 0.9$ at $p < 0.05$): Ga–Al, Cr–Al, Hf–Th.

Note that all elements exhibited better intercorrelations in spring compared to other seasons (Table S2).

3.2 Lake freezing during the glacial period (October to the end of May) and ice-layered structure formation

Observations during the beginning of the ice formation (October 2013) yielded important and novel features of thermokarst lake ice cover evolution during glacial periods. Given the closed basins of all sampled lakes underlain by permafrost without a connection to the groundwater source (i.e., Pokrovsky et al., 2011, 2014), the water was expected to be under excess pressure under the ice. This was confirmed by direct observations in October: the water always rose upward and spread over the ice surface

BGD
12, 1975–2019, 2015

after drilling the first 10–20 cm of the ice layer. Upon the thickening of the ice, cracks formed on the ice cover and the water from the deeper layers seeped and spread over the ice surface, thus forming organic- and Fe-rich multilayered ice up to 30 cm thick. The wind acting on still unfrozen freshly ejected water created ice ripples spreading over a surface of 10–50 m^2 (Fig. S3). The full freezing of ejected organic-rich water led to browning of the ice and presumably produced significant coagulation of colloids. The products of this coagulation could be notably seen at the end of the spring, during massive ice melt (Fig. S4).

In situ oxygen analysis with a submersible O_2 sensor in June and August demonstrates saturation with atmospheric oxygen close to 90 ± 10 %. In October, under the ice, we found only 40–80 % saturation of the water layer, with some redox stratification within 20–50 cm of the unfrozen water column. Generally, the smaller the water body, the lower the oxygen concentration, although a straightforward relation between the size of the lake and the oxygen saturation in October could not be established.

The ice core analysis with the resolution of 5–10 cm demonstrated either an enrichment of the surface ice layers in dissolved elements, or their non-systematic variation over the full depth of the ice core (Table S3). The enrichment, by a factor of 2 to 5, of the first 0 – 30 ± 10 cm was detected for DOC and most metals such as Al, Fe, Ni, Co, Cu, Zn, and Pb, as illustrated for selected metals in Fig. 7. Manganese demonstrated the largest variation along the ice core depth. Its concentration decreased from 3 to 10 ppb at the very surface down to less than 0.1 ppb below 50 cm in depth. In contrast, many trace elements (Cd, Cs, Sb, Ti, Zr, Hf, Th, U, and REEs) did not demonstrate a statistically significant ($p < 0.05$) trend of concentration with depth for three sampled ice cores. Ca^{2+}, SO_4^{2-}, DIC, Cl^-, and Na^+ also demonstrated nonsystematic variation with depth. In winter, only three sampled lakes yielded the liquid water presence above the sediment. The thickness of the unfrozen layer ranged from 10 to 20 cm, with an ice thickness of 60 to 80 cm.

BGD
12, 1975–2019, 2015

Using the element concentration measured in the remaining water at the sediment–ice interface and the bottom 10 cm layer of the ice core, element distribution coefficients between the ice and the remaining fluid can be assessed. The agreement in K_d (water/ice) between three sampled lakes for which both fluid and bottom ice were available is reasonably good for a number of major elements, as can be seen from the average with 2 SD ($n = 3$) listed in Table 2. The lowest K_d (water/ice) is observed for DIC (1.64 ± 0.37) and Cl (7.6 ± 3.0). The DOC distribution varied significantly among the lakes (K_d (water/ice) is between 5 and 21). Al, Ti, Mn, Ce and some REE yielded K_d (water/ice) between 50 and 100. The majority of the other trace elements exhibit K_d (water/ice) between 10 and 40, without any discernable link to element chemical properties and degree of binding to DOM.

The most significant transformation of the lake water chemical composition presumably occurs during the full freezing of the water column over the winter period. At the end of the winter, during massive snowmelt, products of colloidal coagulation are largely present at the surface of the ice blocks within the lake borders (Fig. S4). The coagulates collected in large ($\sim 10^6$ m^2) thermokarst lakes in early June are essentially composed of iron oxy(hydr)oxide and organic matter with significant numbers of co-precipitated trace elements. The aggregates are XRD amorphous and contain 17.5 ± 0.5 % of POC.

Based on total chemical analysis of solid co-precipitates, we calculated the distribution coefficients of the trace element (TE) between the Fe-rich coagulates and the lake water, normalized to Fe (as the major component of the coagulates):

$$K_d = \frac{[TE]/[Fe]_{coagulate}}{[TE]/[Fe]_{lake\ water}},$$

where $[TE]/[Fe]_{lake\ water}$ represents the ratio of average TE and Fe concentrations in large lakes at the end of summer, before the beginning of ice formation. The K_d values of major and trace elements range from 0.05 to 0.5 (Fig. 8). The values of the distribution coefficient obtained in the present study are in reasonable agreement with

BGD
12, 1975–2019, 2015

those reported for colloids (1 kDa–0.45 µm) and the LMW (< 1 kDa) fraction of another large thermokarst lake located in a discontinuous permafrost zone (Pokrovsky et al., 2011), as well as the rivers and streams of the boreal non-permafrost zone (Vasyukova et al., 2010). For the majority of dissolved elements, the K_d of particles are within a factor of 2 different from the previously reported K_d of colloids.

3.3 Seasonal trend in element concentration in the thermokarst lake water: progressive increase from June to February

The first statistical test aimed to assess the difference in element concentrations between different seasons for the full range of the lake size. It was found, using the H criterion of the Kruskal–Wallis and Mann–Whitney U tests, which allowed one to estimate the difference between two independent sets of data based on one given parameter, that all elements are different between the three main seasons at the significance level of $p < 0.05$. This allowed one to calculate the average element concentration with $\pm 2\sigma$ standard deviation for all studied lake sizes from 100 to $> 500\,000\,m^2$ for spring, summer and autumn, as listed in Table 3. Note that the winter data are of low representativity, given that only three unfrozen lakes could be used for this calculation. The median was similar to the average within the 2σ standard deviation of the average.

The majority of dissolved elements exhibited a statistically significant increase in their average concentration from spring to autumn (20–50 %). These are DOC, Mg, K, Ca, Al, Ti, V, Cr, Mn, Fe, Ni, Co, Cu, Ga, Rb, Sr, As, Cd, Sb, Mo, Cs, Ba, all REEs, Pb, and U. Examples of the average element concentration evolution grouped by several families of elements with similar chemical properties and affinity with DOC and Fe colloids (i.e., Pokrovsky et al., 2013) are shown in Fig. 9. The trends of element concentration in the lake water from spring to autumn are quite similar for large ($> 500\,000\,m^2$) and medium ($100–500\,000\,m^2$) water bodies. A conservative scenario of element concentration evolution in thermokarst lakes can be modeled assuming an average lake depth of 75 ± 25 cm in summer, 20 cm flooding in spring, 20 cm ice formation in October and

BGD
12, 1975–2019, 2015

almost full freezing (10 cm of bottom water left) in February. The concentration factor thus calculated is equal to 1, 1.3, 2.0 and 9.5 for spring, summer, autumn and winter, respectively. Conservative behavior of selected major and trace elements is illustrated in Fig. 9 as a dashed line. Most major elements (Si, K) and a number of trace metals (Al, Ti, Cr, Cu) exhibited close to conservative behavior. In contrast, DOC demonstrated significant depletion during winter, between October and February. Fe, Ni, Cd and Pb were slightly non-conservative, showing a depletion in winter.

The effect of the season can be quantified as the ratio of the average summer and autumn to spring concentration ($R_{summer/spring}$). This ratio is the highest for Ba (6.7) and light REEs (7 to 3), followed by Zn (4.3), Si (4.3), Al, Fe and trivalent hydrolysates (4.2 to 2.8), tetravalent hydralysates, Cr and divalent heavy metals such as Co, Cu, Ni, Cd, and Mn (2.5 to 3.3). A number of elements did not demonstrate a significant increase in the concentration during the baseflow season compared to the spring period, exhibiting $R_{summer/spring}$ values below 2 (B, Mg, Na, Ca, Cs, Pb, V, As, Sb, Th and Zr).

Despite significant uncertainty in the average summer-period element concentration in thermokarst lakes (see Table 3), the values obtained in the present study are consistent with thermokarst lake water chemical composition across the gradient of the permafrost zone, from discontinuous/sporadic to continuous permafrost. The values of DOC and all major and trace element concentrations agree, within the uncertainty of the average, with the values of element concentration interpolated from the latitude–lake water concentration dependence (Manasypov et al., 2014) for the latitude of the study site.

3.4 Water residence time effect on lake water chemical composition

The effect of lake water residence time (WRT) on the summer-period and average spring–autumn chemical composition of thermokarst lakes exhibits two clusters of data points (Fig. 10). Statistical analysis of observed dependencies confirmed a significant link between the water residence time and both summer and season-average DOC concentrations with the Spearman correlation coefficient (R_S) equal to

BGD
12, 1975–2019, 2015

−0.65 ($p < 0.05$). The most important result is that, at WRT < 8 months, an almost five-fold increase in DOC concentration occurs. A similar impact is observed for Fe with $R_S = -0.55$ ($p < 0.05$). This result can be understood given that the Fe is likely to be present in the form of organic colloids. The alkaline and alkaline–earth major cations and other metals, however, did not demonstrate any statistically significant ($p > 0.05$) link to the WRT. The estimation of WRT for the smallest (< 10–100 m^2) water bodies was impossible due to the ephemeral nature of these small thaw ponds. However, considering their typical existence between the start of the snowmelt (May) and summer drought (July–August), the water resides in these water bodies between 0.1 and 0.3 years. The highest concentration of DOC observed in spring in < 10 m^2 depressions is therefore consistent with the trend shown for large lakes in Fig. 10.

4 Discussion

4.1 Lake water composition control by snow and ice thaw in spring

The lack of a trend of DOC and metal concentrations with the lake surface area increase above 10 m^2 (Figs. 2–4, S2) in spring implies that the lakes are essentially influenced by allochthonous (surface runoff from thaw snow) sources of dissolved material, with minimal transformation of DOC and metal complexes by intra-lake autochthonous processes. In the opposite case, one would expect a tendency of DOC and chemical element increase with the decrease in the size of the water body, notably below 100 m^2, as it is encountered in summer periods in sporadic and discontinuous permafrost zone of thermokarst lake development (Shirokova et al., 2013). Given that the upper part of the peat column is still frozen at the beginning of June, this source of the solutes to the lake water is most likely to be ground vegetation, comprising dwarf shrubs, mosses and lichens, as well as the litter fall of the previous year. The input of the vegetation leaching products should be similar for the lakes of different sizes, given the very homogeneous palsa bog dominant landscape at the study site.

BGD
12, 1975–2019, 2015

The spring flood period is known to be the most important in terms of land coverage by water, on the annual scale (Zakharova et al., 2009, 2014). As a result, the average chemical composition of the dominant surface waters in the discontinuous permafrost zone of western Siberia can be approximated by that of the spring period as listed in Table 3. Elevated DOC concentration in thermokarst lakes during the spring period, a factor of 2 to 3 higher than the typical 10–15 mg L^{-1} of boreal waters (Dillon and Molot, 1997), suggests high potential for releasing CO_2 into the atmosphere, notably in numerous small depressions filled by thaw water.

A systematic increase in the slope of dependence $UV_{280\,nm}$–[DOC] in the course of the season, from 0.023 in spring to 0.063 in winter, suggests an increase in the input of aromatic compounds (presumably from peat lixiviation) to the end of the vegetative season relative to the leaching of fresh vegetation products (low aromatic, plant and litter exudates) mostly visible after the snowmelt; then, the surrounding peat is still frozen. The lack of any trend in the UV/DOC ratio as a function of the lake size (Fig. 3) strongly suggests the similarity of the DOC sources in the full range of the lake size in each season. As a result, the season rather than the lake size at $S > 100\,m^2$ seems to be the most important factor controlling both the average concentration and the chemical nature of DOC and related elements.

4.2 Concentration mechanism during freezing period; enhanced colloidal coagulation

The unusual distribution of organic carbon and related trace elements over the ice core profile, with an accumulation in the upper 20–40 cm of the ice column, stems from a sequence of events during lake freezing linked to (i) shallow depth and the possibility of the full freezing of the water column and (ii) the lack of any outlet or hydraulic connection to the groundwater of these confined water bodies underlain by the impermeable permafrost layer in the form of the frozen sand/peat. The hypothetical scheme of the crystallization process is illustrated in Fig. 11. The squeezing of the remaining water from the bottom towards the surface through the ice cracks starts

BGD
12, 1975–2019, 2015

as early as October. This produces the layered and organic- and Fe-rich secondary (allochthonous) ice that is crystallized at the already frozen lake surface. During winter, the progressive freezing downwards the water column and the decrease in the connectivity between the remaining water and the lake surface bring about the decrease in element concentration in the bottom ice while concentrating solutes in the remaining fluid at the ice–sediment interface. The progressive lake freezing produces layered ice having contrasted content of major and trace elements among different layers, reflecting the full freezing of water pockets formed via seeping of the bottom water at the lake surface. The DOC and many related elements exhibit a general decrease in concentration downward from the ice core. The freezing sequence of the thermokarst lakes contrasts with the freezing of non-permafrost (glacial) lakes, which are generally deeper than 1 m and have an inlet/outlet and underground connection. To which degree the scheme of ice formation suggested for shallow thermokarst lakes in discontinuous permafrost zones can be applied to other, sporadic and continuous permafrost, regions of western Siberia remains unknown. However, given the shallow depths and closed-basin settings of most thermokarst lakes, the extrapolation of obtained ice chemistry data and partitioning coefficients to other thermokarst lakes of western Siberia should be possible.

To our knowledge, the information on TE partitioning between the lake water and the ice for other boreal settings is lacking. The similar range of DOC and many major and trace metal distribution coefficients between the ice and the remaining solution encountered in the present study (Table 2) is remarkable, and contrasts with the recent results of DOM incorporation during sea ice formation (Muller et al., 2013). The latter authors argued that DOM is incorporated into sea ice relatively more than inorganic solutes. In the case of low total dissolved solid (TDS), DOM-rich thermokarst lakes of the present study, the majority of solutes may follow the DOC being present as organic colloids (1 kDa–0.45 µm), as also demonstrated by dialysis experiments (Pokrovsky et al., 2011, 2013).

BGD
12, 1975–2019, 2015

Various physico-chemical processes may be involved in the transformation of solutes and DOM and metal-rich water pockets incorporated in the ice, notably within most of its surface layers. Among them, photoreductive dissolution of iron oxy(hydr)oxide trapped in the ice (i.e., Kim et al., 2010) can occur both in winter and spring, during massive ice thaw. The enrichment of both Fe and Mn in the first 20 cm of the ice column relative to the deeper ice layers (Fig. 7) can certainly promote enhanced reductive dissolution of both Mn (Kim et al., 2012) and Fe (Kim et al., 2010) under ice thaw during polar day in early June. However, the Fe(II) fraction was estimated to be below 10 % in June's lake sampling, as the $LMW_{<1\,kDa}$ fraction containing essentially non-complex Fe^{2+}(aq) was ≤ 5 % of total dissolved Fe. Therefore, oxygenated spring waters and the shallow depths of thermokarst lakes provide favorable conditions for Fe(III) colloid formation in these organic-rich water bodies. Highly non-conservative behavior of DOC during the winter time demonstrating significant depletion in February (Fig. 9a) strongly suggests intensive heterotrophic respiration of DOM under the ice. Alternatively, the DOC could be transformed into POC and precipitated to the lake bottom or be trapped as particles in the growing ice.

During the massive ice thaw, a significant number of coagulated organo-ferric particles remain on the ice surface (Fig. S4) and eventually precipitate to the lake bottom. Although under anaerobic conditions in the thermokarst lake sediments, Fe(III) may be reduced and return to the water column (Audry et al., 2011), the majority of iron oxy(hydr)oxide is likely to remain in the particulate form, thus preventing Fe from moving to the hydrological network during spring floods. We hypothesize that one of the most powerful mechanisms of organic and organo-mineral colloid coagulation in thermokarst water bodies is annual freezing of the whole water column leading to significant concentrations of Fe, C_{org} and related divalent metals and trivalent and tetravalent hydrolysates in the particulate phase. It is remarkable that Fe-normalized distribution coefficients of TE between the organo-ferric coagulates and filtered (< 0.45 µm) lake water (Fig. 8) are of the same order of magnitude as or within a factor of 2 different from the distribution coefficients of TE between Fe-rich colloids (1 kDa–

BGD
12, 1975–2019, 2015

0.45 µm) and $LMW_{<1\,kDa}$ fractions assessed in previous studies in thermokarst lakes (Pokrovsky et al., 2013) and boreal surface streams (Vasyukova et al., 2010). This similarity strongly suggests that the elementary mechanisms of TE incorporation in organic matter-stabilized iron oxy(hydr)oxides include mainly co-precipitation and that it is generally similar for colloids and particles.

4.3 Allochthonous vs. autochthonous processes forming lake water chemical composition

Allochthonous processes forming lake water chemical composition include the input of fresh vegetation products and the leaching of the upper peat layer. At the beginning of the active season, in June, there is a lateral input of thawing snow, reflecting the interaction of water with ground vegetation such as mosses and lichens as well as with the litter fall of the dwarf shrubs from the previous year. During the summer (baseflow) season, there is peat leaching at the lake border via mainly wave abrasion and elements and DOC release from moss and lichen coverage via lateral flow fed by rains.

The DOM entering the lake ecosystem with the snow thaw and surface inflow during summer rain is subjected to two processes of autochthonous transformation during open water period photo- and bio-degradation, most pronounced in June–September. During summer, the productivity of phytoplankton including possible exometabolite release represents less than 10 % of heterotrophic bacterioplankton respiration in western Siberian thermokarst lakes of the discontinuous/sporadic permafrost zone (Shirokova et al., 2013). The heterotrophic bacterioplankton activity brings about the conversion of colloidal DOM and low molecular weight (LMW) organic ligands to particulate organic matter (POM) in the form of coagulates or the bacterioplankton biomass; in both forms, the POM is likely to precipitate to the lake bottom in the course of the active season. During the glacial period, the processes leading to sedimentation of POC to the lake bottom are cryoconcentration and colloid coagulation (see Sect. 4.2 and Fig. S4). The physico-chemical coagulation of DOC may become

BGD
12, 1975–2019, 2015

especially important during progressive lake freezing in winter. Highly non-conservative behavior of DOC (Fig. 9a) relative to the other major components (Si, K, Na) strongly suggests the preferential removal of DOC from the remaining water under the ice cover. The other elements such as metals Fe, Ni, Cd and Pb (Fig. 9c, i, k, l, respectively) follow non-conservative behavior of DOM, suggesting their massive removal from the water column in the form of organic coagulates. In contrast, Al, Ti, Zn, Cr and Cu (Fig. 9d, e, g, h, j, respectively) remain conservatively in the bottom water or even accumulated in the water. It is possible that they are less dependent on large-size DOM colloids mostly subjected to coagulation during cryoconcentration. It is possible that these metals may be bound to $LMW_{<1\,kDa}$ organic complexes and thus remain in unfrozen water in the lake bottom layer. Additional input of Al and Ti from mineral clayey sediments of the lake (i.e., Audry et al., 2011) cannot be excluded.

The behavior of DIC is almost conservative during lake freezing, without any excess of DIC over the theoretical value in February. As a result, there is no significant accumulation of inorganic carbon in the form of CO_2 or HCO_3^- under the ice cover. This result strongly suggests the dominance of physico-chemical coagulation rather than microbial respiration in DOC removal from the water column in winter. The latter process dominates the spring open water period, when heterotrophic aerobic bacterioplankton respiration of allochthonous DOM produces gaseous CO_2 that is released into the atmosphere in western Siberia thermokarst lakes (Shirokova et al., 2009, 2013), similar to that of the other boreal lakes (Jansson et al., 2008; Rautio et al., 2011). The response of this microbial process to the DOC input in the lake may be very fast, on a matter of days, given that (i) we observed elevated ($> 20\,mg\,L^{-1}$) DOC concentrations in the smallest ($< 2\,m^2$) ground depressions formed within hours after snowmelt, and that (ii) the leaching of DOM from plant litter is very fast (Berg, 2000; Fraysse et al., 2010).

A plot of DOC concentration vs. water residence time in medium and large lakes (300–1 200 000 m^2) revealed two clusters of the data points, with maximal DOC concentration observed in lakes and ponds of short-term water circulation and a stable

BGD
12, 1975–2019, 2015

and rather low DOC concentration ($10 \pm 5\,mg\,L^{-1}$) in lakes of slow water turnover (Fig. 10a). Since the allochthonous input increases DOC in the water body and autochthonous microbial respiration and physico-chemical coagulation remove DOC from the water column, the former process is certainly dominant for short-lived water bodies. The hydrological balance of the smallest water depressions ($< 200\,m^2$) could not be assessed quantitatively, but it can be suggested that the lowest water residence time in these, partially ephemeral, water bodies is consistent with the highest DOC measured in this study. In the lakes of slow water turnover, the input and removal of DOC are presumably balanced. Note, however, the similarity of the intensity of autochthonous processes in larger lakes (i.e., $\geq 100\,000\,m^2$), regardless of their size and the water residence time.

4.4 Consequences for stock of carbon and TE and GHG exchange with the atmosphere over annual scale

The average of the six smallest ($< 1\,m^2$) depressions sampled in spring demonstrates a factor of 2.3 ($p < 0.05$) higher concentration of dissolved organic carbon ($30.8 \pm 7.3\,mg\,L^{-1}$) compared to the larger water bodies ($13.2 \pm 6.6\,mg\,L^{-1}$) during this period. This strongly suggests the importance of short-term plant debris (litter) and submerged ground vegetation leaching by thaw snow, occurring right after the snowmelt. On the western Siberia lowland, the water stock is highest during the spring period, notably in terms of water coverage of the land depressions (60–70 % of the overall watershed area, Zakharova et al., 2014). According to satellite observations in western Siberia, the area subjected to the spring flood period is 55–65 % higher than that of the summer period (Zakharova et al., 2014). Taking into account these observations, and the DOC concentration in thermokarst water bodies, we estimate that the overall increase in soluble stock of DOC and related metals in surface waters in June relative to August may be as high as 200–500 %. This value stems from (i) a factor of 2–3 increase in the wetland flooding in June compared to the summer baseflow season multiplied by

BGD
12, 1975–2019, 2015

(ii) a factor of 1.5–2 higher DOC and metal concentrations in small ($< 1 - 10\,m^2$) water bodies compared to the larger lakes. This dissolved fraction may be easily mobilized from the watershed to the river and further transported to the ocean.

In shallow thermokarst lakes, progressive ice thaw from the surface towards the bottom slowly liberates inorganic carbon trapped or dissolved in the ice. The K_d (water/ice) for DIC (1.2–2.2) is much lower compared to other elements including DOC. As such, the ice is not particularly enriched in DIC relative to the bottom water, and both winter and spring period DIC and CO_2 concentrations are not significantly higher than those in summer. Therefore, we do not expect significant buildup of CO_2 under ice and CO_2 release from the lake water to the atmosphere during spring melt, contrasting with well-known phenomena in deep boreal lakes (Karlsson et al., 2013). Altogether these arguments suggest that the only mechanism capable of enriching the lake water with CO_2 during spring melt is heterotrophic respiration of "fresh" allochthonous DOM, as confirmed by elevated DOC concentrations during this period, notably in small water bodies.

5 Conclusions

A year-round hydrochemical study of shallow thermokarst lakes from a discontinuous permafrost zone of western Siberia revealed conceptually new features of element concentration evolution over different seasons within a large scale of the lake size. Statistical treatment demonstrated that there is no significant difference in element concentration as a function of the lake size within the range of 2×10^2–$2 \times 10^6\,m^2$ in June, August and October. However, in spring, there was a clear increase in DOC and related metal concentrations with the decrease in the size of small water bodies ($< 200\,m^2$). Most of the dissolved elements and organic carbon decreased their concentration following the order June < August < October, regardless of the lake size range, from 2×10^2 to $2 \times 10^6\,m^2$. Therefore, although there are statistically significant differences in organic carbon, major and trace element concentrations

BGD
12, 1975–2019, 2015

between different seasons, the lake size has a negligible influence on the lake water chemical composition, except in very small water bodies. The water residence time (WRT) may be an important parameter controlling lake DOC and Fe concentrations, especially for short-lived water bodies, mostly present during spring. In contrast, the other major and trace elements did not demonstrate any clear link with WRT in the lake.

The ice formation in October created an excessive pressure within the confined water body; the remaining organic- and Fe-rich water was seeping onto the ice surface via cracks of the ice cover. This seeping produced the ice of multiple layers with significant enrichment in Fe, DOC and trace elements in the frozen water pockets within the first 0–20 cm in depth.

Massive coagulation of organo-ferric colloids occurred during full freezing of the lake water and produced macroscopic and organic- and Fe-rich amorphous particles capable of precipitating to the lake bottom. The main mechanisms of element differentiation during ice formation are concentration and coagulation of organic and organo-mineral colloids, as shown by highly non-conservative behavior of DOC and related metals. The partitioning coefficients of TE between the lake water (< 0.45 µm) and the particulate coagulates reflecting the degree of element differentiation during ice formation and full water column freezing were similar to those measured for Fe-rich colloids (1 kDa–0.45 µm) in other thermokarst and boreal lakes and rivers.

The spring flood period created the highest stock of dissolved allochthonous DOC and related metals, notably in small (< 200 m^2) water bodies and depressions. The water dilution during this period (e.g., typically 20 % of the water volume increase) can compete with the increase in the land surface coverage for the overall element stock in lakes in June relative to August. We estimate that the overall increase in soluble stock of DOC and related metals in surface waters and, consequently, potential for river water feeding by lakes during spring floods, ranged from a factor of 2–5. Further assessment of this increase requires high-resolution (< 0.5–1 m^2) remote sensing observation coupled with in situ hydrochemical measurements. Given significant coverage of the

BGD
12, 1975–2019, 2015

land surface by thaw water in spring and elevated DOC concentrations during this period, the overall impact of snowmelt on CO_2 emissions into the atmosphere may be significantly higher compared to that in summer. In contrast, the winter time period leading to full freezing of the water column is unlikely to build up significant GHG concentrations under the ice and appreciably affect the gas regime of thermokarst lakes on the annual scale.

The Supplement related to this article is available online at doi:10.5194/bgd-12-1975-2015-supplement.

Acknowledgements. This work was supported by BIO-GEO-CLIM grant no. 14.B25.31.0001 of the Russian Ministry of Science and Education and by ANR Arctic Metals.

References

Audry, S., Pokrovsky, O. S., Shirokova, L. S., Kirpotin, S. N., and Dupré, B.: Organic matter mineralization and trace element post-depositional redistribution in Western Siberia thermokarst lake sediments, Biogeosciences, 8, 3341–3358, doi:10.5194/bg-8-3341-2011, 2011.

Berg, B.: Litter decomposition and organic matter turnover in northern forest soils, Forest Ecol. Manag., 133, 13–22, 2000.

Boike, J., Kattenstroth, B., Abramova, K., Bornemann, N., Chetverova, A., Fedorova, I., Fröb, K., Grigoriev, M., Grüber, M., Kutzbach, L., Langer, M., Minke, M., Muster, S., Piel, K., Pfeiffer, E.-M., Stoof, G., Westermann, S., Wischnewski, K., Wille, C., and Hubberten, H.-W.: Baseline characteristics of climate, permafrost and land cover from a new permafrost observatory in the Lena River Delta, Siberia (1998–2011), Biogeosciences, 10, 2105–2128, doi:10.5194/bg-10-2105-2013, 2013.

Dillon, P. J. and Molot, L. A.: Dissolved organic and inorganic carbon mass balances in central Ontario lakes. Biogeochemistry, 36, 29–42, 1997.

BGD
12, 1975–2019, 2015

Fraysse, F., Pokrovsky, O. S., and Meunier, J.-D.: Experimental study of terrestrial plant litter interaction with aqueous solutions, Geochim. Cosmochim. Ac., 74, 70–84, 2010.
Grosse, G., Jones, B., and Arp, C.: Thermokarst lakes, drainage, and drained basins. In: Treatise on Geomorphology, edited by: Shroder, J. (Editor in Chief), Giardino, R., Harbor, J., Academic Press, San Diego, CA, Vol. 8, Glacial and Periglacial Geomorphology, 325–353, 2013.
Jansson, M., Hickler, T., Jonsson, A., and Karlsson, J.: Links between terrestrial primary production and bacterial production and respiration in lakes in a climate gradient in subarctic Sweden. Ecosystems, 11, 367–376, 2008.
Karlsson, J., Giesler, R., Persson, J., and Lundin, E.: High emission of carbon dioxide and methane during ice thaw in high latitude lakes, Geophys. Res. Lett., 40, 1123–1127, 2013.
Karlsson, J. M., Lyon, S. W., and Destouni, G.: Thermokast lake, hydrological flow and water balance indicators of permafrost change in Western Siberia, J. Hydrol., 464–465, 459–466, 2012.
Karlsson, J. M., Lyon, S. W., and Destouni, G.: Temporal behavior of lake size-distribution in a thawing permafrost landscape in Northwestern Siberia, Remote Sensing, 6, 621–636, 2014.
Kim, K., Choi, W., Hoffmann, M. R., Yoon, H.-I., and Park, B.-K.: Photoreductive dissolution of iron oxides trapped in ice and its environmental implications, Environ. Sci. Technol., 44, 4142–4148, 2010.
Kim, K., Yoon, H.-I., and Choi, W.: Enhanced dissolution of manganese oxide in ice compared to aqueous phase under illuminated and dark conditions, Environ. Sci. Technol., 46, 13160–13166, 2012.
Kirpotin, S. N., Polishchuk, Y. M., Zakharova, E., Shirokova, L., Pokrovsky, O., Kolmakova, M., and Dupré, B.: One of possible mechanisms of thermokarst lakes drainage in West-Siberian North. Int. J. Environ. Stud., 65, 631–635, 2008.
Laurion, I., Vincent, W. F., MacIntyre, S., Retamal, L., Dupont, C., Francus, P., and Pienitz, R.: Variability in greenhouse gas emissions from permafrost thaw ponds, Limnol. Oceanogr., 55, 115–133, 2010.
Manasypov, R. M., Pokrovsky, O. S., Kirpotin, S. N., and Shirokova, L. S.: Thermokarst lake waters across the permafrost zones of western Siberia, The Cryosphere, 8, 1177–1193, doi:10.5194/tc-8-1177-2014, 2014.

BGD
12, 1975–2019, 2015

Muller, S., Vahatalo, A. V., Stedmon, C. A., Granskog, M. A., Norman, L., Aslam, S., Underwood, G. J. C., Dieckmann, G. S., and Thomas, D. N.: Selective incorporation of dissolved organic matter (DOM) during sea ice formation, Mar. Chem., 155, 148–157, 2013.
Negandhi, K., Laurion, I., Whiticar, M. J., Galand, P. E., Xu, X., and Lovejoy, C.: Small thaw ponds: An accounted source of methane in the Canadian high Arctic, Plos One, 8, e78204, 2013.
Pokrovsky, O. S., Shirokova, L. S., Kirpotin, S. N., Audry, S., Viers, J., and Dupré, B.: Effect of permafrost thawing on organic carbon and trace element colloidal speciation in the thermokarst lakes of western Siberia, Biogeosciences, 8, 565–583, doi:10.5194/bg-8-565-2011, 2011.
Pokrovsky, O. S., Shirokova, L. S., Kirpotin, S. N., Kulizhsky, S. P., and Vorobiev, S. N.: Impact of western Siberia heat wave 2012 on greenhouse gases and trace metal concentration in thaw lakes of discontinuous permafrost zone, Biogeosciences, 10, 5349–5365, doi:10.5194/bg-10-5349-2013, 2013.
Pokrovsky, O. S., Shirokova, L. S., and Kirpotin, S. N.: Biogeochemistry of Thermokarst Lakes of Western Siberia, Nova Science Publ. Inc., NY, 163 pp., 2014.
Rautio, M., Dufresne, F., Laurion, I., Bonilla, S., Vincent, W. F., and Christoffersen, K.: Shallow freshwater ecosystems of the circumpolar Arctic, Ecoscience, 18, 204–222, 2011.
Roach, J., Griffith, B., Verbyla, D., and Jones, J.: Mechanisms influencing changes in lake area in Alaskan boreal forest, Glob. Change Biol., 17, 2567–2583, 2011.
Shirokova, L. S., Pokrovsky, O. S., Kirpotin, S. N., and Dupré, B.: Heterotrophic bacterioplankton in thawed lakes of the northern part of Western Siberia controls the CO_2 flux to the atmosphere, Int. J. Environ. Stud., 66, 433–445, 2009.
Shirokova, L. S., Pokrovsky, O. S., Viers, J., Klimov, S. I., Moreva, O. Yu., Zabelina, S. A., Vorobieva, T. Ya., and Dupré, B.: Diurnal variations of trace metals and heterotrophic bacterioplankton concentration in a small boreal lake of the White Sea basin, Ann. Limnol.-Int. J. Lim., 46, 67–75, 2010.
Shirokova, L. S., Pokrovsky, O. S., Kirpotin, S. N., Desmukh, C., Pokrovsky, B. G., Audry, S., and Viers, J.: Biogeochemistry of organic carbon, CO_2, CH_4, and trace elements in thermokarst water bodies in discontinuous permafrost zones of Western Siberia, Biogeochemistry, 113, 573–593, 2013.
Stepanova, V. M., Pokrovsky, O. S., Viers, J., Mironycheva-Tokareva, N. P., Kosykh, N. P., and Vishnyakova, E. K.: Major and trace elements in peat profiles in Western Siberia: impact

BGD
12, 1975–2019, 2015

of the landscape context, latitude and permafrost coverage, Appl. Geochem., 53, 53–70, doi:10.1016/j.apgeochem.2014.12.004, 2015.
Tank, S. E., Lesack, L. F. W., Gareis, J. A. L., Osburn, C. L., and Hesslein, R. H.: Multiple tracers demonstrate distinct sources of dissolved organic matter to lakes of the Mackenzie Delta, western Canadian Arctic, Limnol. Oceanogr., 56, 1297–1309, 2011.
Tank, S. E., Esslein, R. H. H., and Lesack, L. F. W.: Northern delta lakes as summertime CO_2 absorbers within the arctic landscape, Ecosystems, 12, 144–157, 2009.
Vasyukova, E. V., Pokrovsky, O. S., Viers, J., Oliva, P., Dupré, B., Martin, F., and Candaudap, F.: Trace elements in organic- and iron-rich surficial fluids of the boreal zone: Assessing colloidal forms via dialysis and ultrafiltration, Geochim. Cosmochim. Ac., 74, 449–468, doi:10.1016/j.gca.2009.10.026, 2010.
Walter, K. M., Zimov, S. A., Chanton, J. P., Verbyla, D., and Chapin III, F. S.: Methane bubbling from Siberian thaw lakes as a positive feedback to climate warming, Nature, 443, 71–75, 2006.
Walter, K. M., Chanton, J. P., Chapin III, F. S., Schuur, E. A. G., and Zimov, S. A.: Methane production and bubble emissions from arctic lakes: Isotopic implications for source pathways and ages, J. Geophys. Res, 113, G00A08, 2008.
Walter Anthony, K. M., Anthony, P., Grosse, G., and Chanton, J.: Geologic methane seeps along boundaries of Arctic permafrost thaw and melting glaciers, Nat. Geosci., 5, 419–426, 2012.
Walter Anthony, K. M. and Anthony, P.: Constraining spatial variability of methane ebullition in thermokarst lakes using point-process models, J. Geophys. Res, 118, doi:10.1002/jgrg.20087, 2013.
Walter Anthony, K. M., Zimov, S. A., Grosse, G., Jones, M. C., Anthony, P. M., Chapin III, F. S., Finlay, J. C., Mack, M. C., Davydov, S., Frenzel, P., and Frolking, S.: A shift of thermokarst lakes from carbon sources to sinks during the Holocene epoch, Nature, 511, 452–456, 2014.
Yeghicheyan, D., Bossy, C., Bouhnik Le Coz, M., Douchet, C., Granier, G., Heimburger, A., Lacan, F., Lanzanova, A., Rousseau, T. C. C., Seidel, J.-L., Tharaud, M., Candaudap, F., Chmeleff, J., Cloquet, C., Delpoux, S., Labatut, M., Losno, R., Pradoux, C., Sivryn, Y., and Sonke, J. E.: A Compilation of silicon, rare earth element and twenty-one other trace element concentrations in the natural river water reference material SLRS-5 (NRC-CNRC), Geostand. Geoanal. Res., 37, 449–467, 2014.

BGD
12, 1975–2019, 2015

Zakharova, E. A., Kouraev, A. V., Kolmakova, M. V., Mognard, N. M., Zemtsov, V. A., and Kirpotin, S. N.: The modern hydrological regime of the northern part of Western Siberia from in situ and satellite observations, Int. J. Environ. Stud., 66, 447–463, 2009.

Zakharova, E. A., Kouraev, A. V., Frédérique, R., Zemtsov, V. A., and Kirpotin, S. N.: Seasonal variability of the Western Siberia wetlands from satellite radar altimetry, J. Hydrol., 512, 366–378, 2014.

BGD

12, 1975–2019, 2015

Table 1. Major hydrophysical and hydrochemical parameters of studied lakes.

	N	E	S, m^2	T, °C	O_2, mg L^{-1}	O_2, % sat	R, µS cm^{-1}	pH	DIC, ppm	DOC, ppm	Cl, ppm	SO_4, ppm
June												
Z-43	63°13,580′	75°43,476′	1.8	6.5	N.D.	N.D.	N.D.	3.43	0.749	22.5	0.1532	0.9452
Z-44	63°13,567′	75°43,465′	0.071	7.5	N.D.	N.D.	N.D.	3.25	0.562	33.9	0.1458	0.9957
Z-45	63°13,559′	75°43,467′	4.9	6.0	N.D.	N.D.	N.D.	3.43	0.784	26.5	0.1466	0.8256
Z-46	63°13,513′	75°43,527′	31 400	7.2	N.D.	N.D.	N.D.	3.28	0.396	13.6	0.0663	0.3680
Z-47	63°13,521′	75°43,608′	1.8	5.5	N.D.	N.D.	N.D.	3.51	0.598	23.6	0.0978	0.5896
Z-48	63°13,492′	75°43,726′	78.5	5.9	N.D.	N.D.	N.D.	3.49	0.433	17.2	0.0306	0.4516
Z-49	63°13,475′	75°43,737′	1.0	5.2	N.D.	N.D.	N.D.	3.37	0.545	22.1	0.1285	0.7087
Z-50	63°13,436′	75°43,707′	96 163	7.5	N.D.	N.D.	N.D.	3.77	0.550	6.5	0.0848	0.4372
Z-51	63°13,492′	75°43,584′	25 434	7.2	N.D.	N.D.	N.D.	3.08	0.435	14.7	0.0131	0.448
Z-52	63°13,505′	75°43,444′	17 663	6.6	N.D.	N.D.	N.D.	3.36	0.390	13.3	0.0678	0.369
Z-53	63°13,512′	75°43,374′	9.6	5.8	N.D.	N.D.	N.D.	3.47	0.447	17.4	0.0289	0.576
Z-54	63°13,521′	75°43,389′	0.13	5.5	N.D.	N.D.	N.D.	3.11	0.855	27.2	0.1337	0.752
Z-56	63°47′55.0″	75°31′21.0″	5671.6	3.8	9.1	86	12	4.2	0.431	14.1	0.1781	0.097
Z-57	63°47′54.4″	75°31′6.55″	3000	5.7	8.86	82	12	4.35	0.423	9.8	0.1637	0.616
Z-58	63°47′56.5″	75°31′19.9″	314	6.2	8.19	79	13	4.4	0.438	10.2	0.1616	0.595
Z-59	63°47′56.2″	75°31′14.8″	5024	6.0	8.3	77	30	4.5	0.437	24.9	0.0501	0.476
Z-60	63°47′55.0″	75°31′14.1″	314.	6.6	8.23	78	21	4.0	0.459	15.2	0.0657	0.301
Z-61	63°47′56.1″	75°31′12.9″	176.6	6.5	8.2	77	17	4.05	0.410	12.5	0.0809	0.589
Z-62	63°48′28.0″	75°30′52.1″	1 766 250	5.9	8.25	79	12	4.2	0.477	13.	0.2440	0.843
Z-63	63°48′04.7″	75°31′13.4″	28.3	8.5	7.33	74	20	4.5	0.394	24.5	0.024	0.233
Z-64	63°48′05.0″	75°31′14.5″	19.6	10.5	8.54	88	23	4.3	0.524	24.4	0.040	0.615
Z-65	63°48′29.5″	75°30′50.5″	11 304	8.3	8.6	86	14	4.4	0.449	17.1	0.157	0.731
Z-66	63°48′00.2″	75°30′53.8″	314.	9.9	8.55	85	15	4.8	0.429	12.6	0.064	0.964
Z-67	63°47′59.3″	75°30′46.8″	78.5	11.4	8.38	90	28	5.01	0.402	18.8	0.050	0.385
Z-68	63°47′59.0″	75°30′46.8″	176.6	10.2	8.46	88	22	4.4	0.378	16.9	0.043	0.725
Z-69	63°47′58.7″	75°30′48.8″	314.	8.5	9.2	99	14	3.9	0.458	12.9	0.149	0.341
Z-70	63°47′58.0″	75°30′48.3″	78.5	12.5	8.25	91	18	4.7	0.378	17.9	0.040	0.505
Z-71	63°47′58.9″	75°30′47.9″	0.0079	N.D.	N.D.	N.D.	N.D.	N.D.	0.610	22.6	1.484	0.843
Z-72	63°48′04.5″	75°30′43.7″	1.8	16.5	7.5	84	30	3.92	0.390	18.2	0.170	0.860
Z-73	63°48′15.5″	75°31′07.4″	706.5	12.9	8.7	98	17	3.8	0.372	12.8	0.069	0.339
Z-74	63°48′39.7″	75°31′59.9″	176 625	6.3	9.2	94	9	4.0	0.426	7.8	0.146	0.647
Z-75	63°48′39.9″	75°31′59.4″	0.2	17.2	8.1	82	34	3.7	0.854	35.4	0.102	0.776
Z-77	63°46′58.0″	75°39′12.2″	113	12.4	7.95	87	32	4.4	0.432	27.5	0.102	0.247
Z-78	63°47′01.4″	75°39′14.0″	3.1	10.8	7.12	77	41	3.7	0.419	27.7	0.037	0.419
Z-79	63°47′01.0″	75°39′05.4″	314	12.7	7.6	86	18	3.5	0.304	18.3	0.022	0.201
Z-80	63°46′56.6″	75°39′13.1″	1256	11.8	7.8	85	23	3.3	0.303	19.4	0.093	0.276
Z-81	63°47′01.7″	75°39′02.2″	31 400	12	8.3	93	19	4.0	0.323	15.8	0.304	0.163
Z-82	63°47′07.2″	75°39′02.0″	113	14.4	8.4	97	19	4.2	0.359	15.3	0.009	0.216
Z-83	63°47′18.9″	75°38′30.1″	1 766 250	3.4	8.6	82	11	4.6	0.858	6.5	0.117	0.209
Z-84	63°47′06.7″	75°38′10.8″	314	15.1	7.8	9	19	3.9	0.355	17.2	0.009	0.244
Z-85	63°47′05.4″	75°38′10.4″	70 650	1.9	7.99	8	7	4.6	0.433	5.5	0.067	0.471
Z-87	63°47′41.5″	75°33′01.0″	1256	13.7	8.43	95	12	4.5	0.338	11.6	0.060	0.493
Z-88	63°47′43.9″	75°33′07.5″	177	2.5	8.02	98	N.D.	4.6	0.325	17.9	0.031	0.260
Z-89	63°47′44.2″	75°33′09.0″	707	N.D.	7.4	98	N.D.	N.D.	0.285	9.7	0.189	0.215
Z-90	63°47′45.5″	75°33′09.7″	159	N.D.	7.9	95	N.D.	N.D.	0.283	12.1	0.138	0.146
Z-91	63°47′49.2″	75°33′10.3″	380	N.D.	7.8	95	23	4.4	0.329	25.3	0.045	0.247
Z-92	63°48′01.0″	75°33′28.5″	78.5	20	7.7	95	12	4.7	0.334	16.6	0.014	0.255
Z-93	63°48′11.0″	75°33′54.4″	2 268 650	16	8.36	99	9	4.8	0.402	18.5	0.245	0.756
Z-94	63°48′16.8″	75°33′47.2″	19.6	18	8.36	104	24	3.9	0.304	20.2	0.041	0.272
Z-95	63°48′29.7″	75°33′55.0″	4.9	17.8	7.4	98	31	4.1	0.305	26.	0.045	0.732
Z-96*	63°48′30.2″	75°33′54.7″	580 586	9.3	7.9	88	8	4.7	0.550	8.6	0.166	1.011
Z-97	63°47′39.0″	75°33′02.3″	3	19.6	7.9	91	18	4.34	0.285	21.9	0.032	0.316
Z-98	63°46′17.2″	75°40′58.6″	0.79	15.6	7.27	92	19	4.5	0.282	20.7	0.108	0.317
Z-99	63°46′18.5″	75°40′42.9″	314	17.9	6.44	86	N.D.	4.45	0.298	20.3	0.136	0.027
Z-100	63°46′14.4″	75°40′34.2″	3.1	15.7	6.7	84	N.D.	4.15	0.311	23.7	0.081	0.322
Z-101	63°46′14.4″	75°40′32.5″	785	13.3	6.8	8	N.D.	4.0	0.347	10.	0.055	0.252
Z-102	63°46′10.1″	75°40′21.5″	4.9	12.5	5.7	7	N.D.	3.6	0.353	28.8	0.151	0.465
Z-103	63°46′09.2″	75°40′11.4″	961.6	19.5	6.8	88	N.D.	4.2	0.291	20.9	0.075	0.318
Z-104	63°46′07.8″	75°40′07.0″	0.13	17.9	5.3	71	N.D.	3.6	0.304	45.	0.182	0.619
Z-105	63°46′07.7″	75°40′04.4″	706.5	14.6	6.7	80	N.D.	4.2	0.294	18.4	0.037	0.218
Z-106	63°46′01.4″	75°39′57.0″	12.6	18.2	6.8	90	N.D.	4.1	0.270	22.4	0.043	0.305
Z-107	63°46′03.7″	75°39′54.3″	196 250	15.6	6.8	85	N.D.	4.31	0.293	25.	N.D.0	N.D.

* Asterisk stands for a lake sampled during all four seasons.

BGD
12, 1975–2019, 2015

Table 1. Continued.

	N	E	S, m^2	T, °C	O_2, mg L^{-1}	O_2, % sat	R, µS cm^{-1}	pH	DIC, ppm	DOC, ppm	Cl, ppm	SO_4, ppm
August												
Z-1	63°47′57.9″	75°33′49.2″	**1 200 000**	N.D.	N.D.	N.D.	N.D.	5.45	0.422	16.55	0.089	0.3259
Z-2*	63°48′11.1″	75°33′23.2″	**580 586**	N.D.	N.D.	N.D.	N.D.	5.63	0.440	14.40	0.187	0.6155
Z-3	63°48′27.6″	75°32′29.3″	**51 300**	N.D.	N.D.	N.D.	N.D.	4.88	0.376	13.86	0.111	0.2534
Z-4	63°51′32.11″	75°37′10.6″	**33 000**	N.D.	N.D.	N.D.	N.D.	4.88	0.363	7.73	0.039	0.0804
Z-5	63°49′32.1″	75°34′00.6″	**74 000**	N.D.	N.D.	N.D.	N.D.	4.92	0.429	12.8	0.423	0.1880
Z-6	63°47′15.2″	75°37′58.3″	**138 000**	N.D.	N.D.	N.D.	N.D.	6.20	2.470	11.7	0.480	0.1711
Z-7	63°47′06.7″	75°38′12.2″	**60 000**	N.D.	N.D.	N.D.	N.D.	4.67	0.385	13.7	0.076	0.1023
Z-8	63°47′02.3″	75°38′02.5″	**6000**	N.D.	N.D.	N.D.	N.D.	4.41	0.370	27.7	0.156	0.342
Z-9	63°47′01.1″	75°39′05.5″	**359.8**	N.D.	N.D.	N.D.	N.D.	4.20	0.403	27.4	0.098	0.200
Z-10	63°46′56.8″	75°39′10.9″	**1481.9**	N.D.	N.D.	N.D.	N.D.	4.21	0.334	51.8	0.197	0.326
Z-11	63°46′53.8″	75°39′18.6″	**1 766 250**	N.D.	N.D.	N.D.	N.D.	5.28	0.392	8.4	0.182	0.283
Z-12	63°47′36.2″	75°33′10.0″	**1256**	N.D.	N.D.	N.D.	N.D.	4.66	0.392	11.6	0.048	0.104
Z-13	63°47′38.5″	75°33′07.1″	**1963**	N.D.	N.D.	N.D.	N.D.	4.16	0.570	35.4	0.090	0.306
Z-14	63°47′43.8″	75°33′12.5″	**1963**	N.D.	N.D.	N.D.	N.D.	4.33	0.310	18.5	0.037	0.114
Z-15	63°47′45.9″	75°33′11.2″	**1809**	N.D.	N.D.	N.D.	N.D.	4.19	0.301	19.5	0.038	0.072
Z-16	63°47′49.3″	75°33′10.6″	**201.0**	N.D.	N.D.	N.D.	N.D.	4.16	0.386	35.7	0.077	0.119
Z-17	63°47′56.3″	75°31′26.1″	**2374.6**	N.D.	N.D.	N.D.	N.D.	4.94	0.341	52.9	1.178	0.486
Z-18	63°47′56.6″	75°31′21.9″	**707**	N.D.	N.D.	N.D.	N.D.	4.35	0.373	17.6	0.082	0.049
Z-19	63°47′56.0″	75°31′12.7″	**415**	N.D.	N.D.	N.D.	N.D.	4.17	0.335	23.4	0.088	0.091
Z-20	63°48′00.9″	75°30′54.8″	**78.5**	N.D.	N.D.	N.D.	N.D.	4.65	0.306	38.6	0.242	0.159
Z-21	63°47′58.9″	75°30′50.8″	**491**	N.D.	N.D.	N.D.	N.D.	4.50	0.319	35.6	0.118	0.245
Z-22	63°47′58.2″	75°30′53.8″	**7850**	N.D.	N.D.	N.D.	N.D.	4.25	0.316	31.0	0.157	3.115
Z-23	63°47′56.8″	75°30′43.7″	**4416**	N.D.	N.D.	N.D.	N.D.	4.56	0.300	28.7	0.084	3.116
Z-24	63°47′57.4″	75°30′33.9″	**6359**	N.D.	N.D.	N.D.	N.D.	4.35	0.321	18.9	0.142	0.126
Z-25	63°47′59.3″	75°30′35.1″	**5408**	N.D.	N.D.	N.D.	N.D.	4.88	0.312	18.6	0.073	0.164
Z-26	63°47′57.5″	75°30′30.8″	**314**	N.D.	N.D.	N.D.	N.D.	4.48	0.340	54.7	0.193	0.280
Z-27	63°43′59.9″	75°49′48.3″	**2375**	N.D.	N.D.	N.D.	N.D.	5.88	0.865	9.3	0.031	2.016
Z-28	63°44′12.7″	75°48′55.6″	**3524**	N.D.	N.D.	N.D.	N.D.	6.10	1.251	15.3	0.197	0.183
Z-29	63°47′26.1″	75°33′50.5″	**152**	N.D.	N.D.	N.D.	N.D.	5.54	0.465	22.8	0.766	0.246
Z-30	63°47′28.2″	75°33′51.8″	**31 400**	N.D.	N.D.	N.D.	N.D.	5.59	0.360	38.2	0.608	4.797
Z-31	63°47′42.9″	75°31′32.4″	**5024**	N.D.	N.D.	N.D.	N.D.	5.66	0.357	10.6	0.55	0.855
October												
OZ-1	63°13′31.6″	75°43′32.6″	**96 163**	N.D.	N.D.	N.D.	N.D.	4.21	1.552	48.2	0.181	0.110
OZ-2	63°13′22.6″	75°43′22.1″	**17 663**	N.D.	N.D.	N.D.	N.D.	4.57	0.713	32.1	0.183	0.379
OZ-3	63°13′18.8″	75°43′22.1″	**491**	N.D.	N.D.	N.D.	N.D.	5.29	1.835	52.7	0.282	0.232
OZ-4	63°13′15.1″	75°43′19.0″	**70 650**	N.D.	N.D.	N.D.	N.D.	4.69	0.618	12.3	0.128	0.153
OZ-5	63°13′16.4″	75°43′34.6″	**1963**	N.D.	N.D.	N.D.	N.D.	3.75	0.536	27.5	0.115	0.128
OZ-6	63°13′20.8″	75°43′44.8″	**12 266**	N.D.	N.D.	N.D.	N.D.	4.29	0.445	14.1	0.078	0.133
OZ-7	63°13′16.5″	75°43′17.1″	**49 063**	N.D.	N.D.	N.D.	N.D.	4.99	0.533	13.5	0.129	0.164
OZ-8	63°13′06.5″	75°43′22.4″	**707**	N.D.	N.D.	N.D.	N.D.	4.74	1.828	39.1	0.309	0.308
OZ-9	63°13′03.4″	75°43′15.7″	**2826**	N.D.	N.D.	N.D.	N.D.	4.33	0.488	17.0	0.106	0.037
OZ-10	63°13′23.2″	75°43′02.6″	**177**	N.D.	N.D.	N.D.	N.D.	4.52	3.492	35.4	1.252	0.178
OZ-11	63°47′54.1″	75°31′33.3″	**110**	N.D.	N.D.	N.D.	N.D.	3.99	0.723	24.3	0.541	0.036
OZ-12	63°48′03.0″	75°31′33.8″	**196 250**	N.D.	9.3	86	N.D.	4.57	1.264	29.2	0.201	0.746
OZ-13	63°48′18.2″	75°31′30.4″	**196 250**	N.D.	10.5/8.3	95/74	8	4.77	0.574	24.3	0.165	0.601
OZ-14	63°48′28.0″	75°31′28.7″	**707**	N.D.	12.3/1	100/94	6	4.21	0.460	16.8	0.122	0.060
OZ-15	63°48′36.8″	75°31′38.1″	**41 527**	N.D.	8.8/7.2	74/64	N.D.	4.84	0.650	26.3	0.224	0.248
OZ-16	63°48′37.3″	75°32′28.2″	**567 163**	N.D.	7.4/6.2	67/56	N.D.	4.87	0.581	13.7	0.194	0.314
OZ-17*	63°48′21.0″	75°33′08.6″	**580 586**	N.D.	9.1/6.9	8/66	N.D.	5.01	0.507	15.3	0.284	0.316
OZ-18	63°48′15.2″	75°34′12.0″	**1 326 650**	N.D.	8.1/7.3	8/68	N.D.	4.69	0.495	13.7	0.193	0.708
OZ-19	63°47′52.9″	75°33′19.8″	**9499**	N.D.	8.6/5.8	78/55.2	N.D.	4.10	0.602	29.6	0.074	0.247
OZ-20	63°47′47.0″	75°33′11.3″	**2375**	N.D.	11.7/10.3	101/97	N.D.	4.01	0.596	24.9	0.179	0.052
OZ-21	63°47′47.2″	75°32′58.9″	**11 304**	N.D.	10.1/4.7	92/44	N.D.	4.91	0.530	45.6	0.464	1.410
OZ-22	63°46′56.1″	75°38′53.7″	**2462**	N.D.	8.25/5.87	72/53	N.D.	3.96	0.508	28.6	0.246	1.566
OZ-23	63°46′58.4″	75°38′45.2″	**5024**	N.D.	4.2/3.34	38/30	N.D.	3.81	0.662	27.7	0.828	0.878
OZ-24	63°46′59.0″	75°38′33.8″	**3215**	N.D.	5.1/4.5	46/40	N.D.	3.99	0.595	16.5	0.140	0.121
OZ-25	63°47′02.6″	75°38′21.2″	**3140**	N.D.	9.2/4.4	85/41	N.D.	4.06	0.556	16.3	0.095	0.204
OZ-26	63°47′1.8″	75°38′24.2″	**5672**	N.D.	8.3/4.	75/38	N.D.	4.85	0.820	31.1	0.234	2.909
OZ-27	63°47′12.1″	75°38′34.64″	**17 663**	N.D.	7.8/5.4	79/49	N.D.	3.87	0.466	33.1	0.164	0.535
OZ-28	63°47′21.9″	75°38′28.2″	**785 000**	N.D.	9.75	87	N.D.	6.90	2.920	12.3	0.543	1.686
OZ-29	67°47′1.2″	75°38′51.1″	**28 339**	N.D.	4.2/5.4	37/49	N.D.	3.98	0.488	37.5	0.170	0.606
OZ-30	63°47′04.2″	75°38′56.1″	**13 267**	N.D.	4.2/5.8	37/51	N.D.	3.98	0.444	34.4	0.187	0.669
OZ-31	63°46′57.8″	75°39′02.1″	**962**	N.D.	4.5/3.9	4/35	N.D.	3.77	0.469	23.1	0.229	0.186
February												
LF1 bottom	63°48′19.6″	75°33′19.2″	**580 586**	N.D.	N.D.	N.D.	N.D.	N.D.	0.496	30.3	0.792	3.440
LF4 bottom	63°48′44.7″	75°34′37.3″	**351 335**	N.D.	N.D.	N.D.	19	4.655	0.778	19.0	0.235	1.678
LFS bottom	63°49′09.4″	75°34′44.1″	**1 743 000**	N.D.	N.D.	N.D.	31	4.778	1.022	32.9	0.281	2.973

BGD
12, 1975–2019, 2015

Table 2. Distribution coefficient of soluble components between the lake water and the ice (average of three samples). The lower part of the ice column, formed in quasi-equilibrium with the remaining bottom water, was used for this estimation.

Element	K_d (water)/(ice)
DIC	1.64 ± 0.37
DOC	10.3 ± 7.0
Cl^-	7.58 ± 3.0
SO_4	44.1 ± 10.9
Na	21.2 ± 3.4
Mg	17.9 ± 5.4
Al	93.1 ± 32.9
Si	12.4 ± 5.2
K	45.8 ± 24.1
Ca	10.2 ± 5.2
Ti	50 ± 20
V	22.9 ± 3.5
Cr	20.7 ± 8.9
Mn	117 ± 35
Fe	67.8 ± 12.4
Ni	16.6 ± 2.7
Cu	46.8 ± 21.5
Ga	34.9 ± 12.1
As	46.4 ± 9.8
Rb	41.7 ± 14.4
Sr	20.2 ± 12.7
Cd	7.4 ± 1.7
Sb	10.9 ± 1.9
Cs	5.7 ± 2.1
Ba	27.2 ± 9.3
La	41.3 ± 16.2
Ce	58.8 ± 21.0
Pr	45.8 ± 38.5
Nd	52.4 ± 9.6
Sm	26.7 ± 13.9
Eu	49.0 ± 32.5
Gd	21.6 ± 1.6
Dy	47.5 ± 34.5
Ho	14.4 ± 11.2
Er	23.4 ± 7.9
Yb	19.1 ± 12.4
Pb	41.5 ± 12.2
U	11.5 ± 2.9

BGD
12, 1975–2019, 2015

Table 3. Average concentrations and standard deviation ($\pm 2\sigma$) of major and trace elements during different seasons of the year for two size classes of thermokarst lakes, 100–500 000 m^2 and > 500 000 m^2.

Element	units	100–500 000 m^2				> 500 000 m^2			
		spring	summer	autumn	winter	spring	summer	autumn	winter
DOC	mgL^{-1}	15.2 ± 5.1	25.6 ± 13.3	28 ± 10.9	n.d.	13.2 ± 6.6	12.9 ± 2.8	16.8 ± 6.2	27.4 ± 6.03
DIC	mgL^{-1}	0.38 ± 0.07	0.42 ± 0.2	0.79 ± 0.67	n.d.	0.5 ± 0.18	0.49 ± 0.17	1.15 ± 0.93	0.77 ± 0.21
Cl^-	mgL^{-1}	0.09 ± 0.06	0.13 ± 0.11	0.21 ± 0.16	n.d.	0.18 ± 0.05	0.21 ± 0.14	0.28 ± 0.13	0.44 ± 0.25
SO_4^{2-}	mgL^{-1}	0.37 ± 0.2	0.44 ± 0.41	0.43 ± 0.38	n.d.	0.69 ± 0.27	0.33 ± 0.15	0.75 ± 0.5	2.33 ± 0.65
Specific cond.	μScm^{-1}	17.9 ± 5.98	n.d.	7 ± 1	n.d.	9.8 ± 1.47	n.d.	n.d.	25 ± 6
pH		4.2 ± 0.34	4.72 ± 0.58	4.17 ± 0.38	n.d.	4.44 ± 0.29	5.49 ± 0.44	5.21 ± 0.86	4.72 ± 0.06
Be	μgL^{-1}	0.004 ± 0.001	0.007 ± 0.004	0.013 ± 0.008	n.d.	0.002 ± 0.001	0.012 ± 0.003	0.013 ± 0.005	
B	μgL^{-1}	42.4 ± 41.8	28.7 ± 26.5	76.6 ± 66.3	n.d.	8.22 ± 7.61	30.1 ± 20.3	223 ± 169	776 ± 413
Na	μgL^{-1}	866 ± 854	1220 ± 1197	910 ± 608	n.d.	997 ± 782	896 ± 351	1396 ± 925	6519 ± 3818
Mg	μgL^{-1}	99.5 ± 35	229 ± 186	150 ± 76.6	n.d.	62.2 ± 38.4	125 ± 12.7	199 ± 48.3	316 ± 137
Al	μgL^{-1}	34.7 ± 18.3	101 ± 69.4	181 ± 114	n.d.	41.7 ± 15.4	137 ± 77.7	238 ± 110	484 ± 169
K	μgL^{-1}	124 ± 123	207 ± 203	302 ± 227	n.d.	256 ± 144	272 ± 95.6	447 ± 253	2251 ± 1254
Ca	μgL^{-1}	211.4 ± 92.7	289 ± 160	309 ± 152	n.d.	213 ± 167	470 ± 367	661 ± 438	893 ± 406
Ti	μgL^{-1}	0.512 ± 0.27	1.16 ± 0.664	1.76 ± 1.3	n.d.	0.569 ± 0.229	4.46 ± 2.75	4.44 ± 4.01	3.63 ± 1.24
V	μgL^{-1}	0.272 ± 0.088	0.363 ± 0.252	0.484 ± 0.361	n.d.	0.415 ± 0.205	0.848 ± 0.374	0.882 ± 0.402	1.33 ± 0.298
Cr	μgL^{-1}	0.138 ± 0.075	0.366 ± 0.166	0.477 ± 0.274	n.d.	0.157 ± 0.045	0.457 ± 0.125	0.651 ± 0.238	1.14 ± 0.423
Mn	μgL^{-1}	6.25 ± 4.39	15.7 ± 9.92	14.6 ± 8.95	n.d.	4.14 ± 3.52	17.9 ± 4.02	21.1 ± 8.77	26.3 ± 11.7
Fe	μgL^{-1}	84.4 ± 57.3	251 ± 162	230 ± 111	n.d.	127 ± 63	273 ± 240	336 ± 146	447 ± 108
Co	μgL^{-1}	0.037 ± 0.018	0.103 ± 0.05	0.141 ± 0.064	n.d.	0.029 ± 0.016	0.095 ± 0.035	0.093 ± 0.039	0.215 ± 0.034
Ni	μgL^{-1}	0.108 ± 0.067	0.316 ± 0.149	0.299 ± 0.171	n.d.	0.106 ± 0.04	0.557 ± 0.425	0.351 ± 0.141	0.477 ± 0.145
Cu	μgL^{-1}	0.252 ± 0.207	0.47 ± 0.289	0.789 ± 0.691	n.d.	0.208 ± 0.07	0.634 ± 0.439	1.2 ± 0.768	3.56 ± 2.01
Zn	μgL^{-1}	27.1 ± 23.3	62.2 ± 47	114 ± 97.8	n.d.	27.8 ± 26.2	108 ± 97.3	314 ± 276	794 ± 423
Ga	μgL^{-1}	0.01 ± 0.004	0.023 ± 0.016	0.042 ± 0.033	n.d.	0.007 ± 0.004	0.037 ± 0.023	0.06 ± 0.031	0.146 ± 0.069
As	μgL^{-1}	0.371 ± 0.093	0.636 ± 0.191	0.612 ± 0.288	n.d.	0.371 ± 0.069	0.626 ± 0.057	0.658 ± 0.182	0.944 ± 0.3
Rb	μgL^{-1}	0.147 ± 0.141	0.213 ± 0.205	0.328 ± 0.294	n.d.	0.275 ± 0.069	0.388 ± 0.166	0.92 ± 0.536	2.07 ± 0.963
Sr	μgL^{-1}	2.84 ± 1.42	5.91 ± 3.96	8 ± 5.53	n.d.	3.12 ± 1.6	8.94 ± 4.72	13 ± 6.22	29.5 ± 12.6
Zr	μgL^{-1}	0.243 ± 0.2	0.1 ± 0.068	0.216 ± 0.165	n.d.	0.488 ± 0.011	0.309 ± 0.138	0.612 ± 0.359	2.06 ± 1.8
Nb	μgL^{-1}	0.015 ± 0.011	0.014 ± 0.012	0.024 ± 0.023	n.d.	0.013 ± 0.002	0.024 ± 0.012	0.02 ± 0.015	0.024
Mo	μgL^{-1}	0.012 ± 0.007	0.01 ± 0.009	0.021 ± 0.015	n.d.	0.023 ± 0.008	0.021 ± 0.003	0.021 ± 0.009	0.033 ± 0.017
Cd	μgL^{-1}	0.01 ± 0.007	0.024 ± 0.015	0.028 ± 0.013	n.d.	0.0005	0.017 ± 0.01	0.025 ± 0.019	0.04 ± 0.008
Sb	μgL^{-1}	0.04 ± 0.014	0.046 ± 0.012	0.077 ± 0.031	n.d.	0.037 ± 0.01	0.064 ± 0.015	0.08 ± 0.027	0.14 ± 0.044
Cs	μgL^{-1}	0.008 ± 0.007	0.008 ± 0.007	0.007 ± 0.006	n.d.	0.003 ± 0.002	0.013 ± 0.007	0.023 ± 0.013	0.027 ± 0.011
Ba	μgL^{-1}	49.5 ± 48.9	126.4 ± 81.2	410 ± 393	n.d.	63.5 ± 61.8	139 ± 77.3	466 ± 367	1107 ± 446
La	μgL^{-1}	0.01 ± 0.007	0.037 ± 0.031	0.052 ± 0.041	n.d.	0.003 ± 0.002	0.072 ± 0.02	0.071 ± 0.016	0.221 ± 0.016
Ce	μgL^{-1}	0.021 ± 0.014	0.09 ± 0.083	0.122 ± 0.114	n.d.	0.001 ± 0.0009	0.15 ± 0.052	0.14 ± 0.02	0.561 ± 0.04
Pr	μgL^{-1}	0.004 ± 0.003	0.011 ± 0.01	0.016 ± 0.015	n.d.	n.d.	0.018 ± 0.006	0.017 ± 0.003	0.065 ± 0.007
Nd	μgL^{-1}	0.016 ± 0.011	0.047 ± 0.045	0.059 ± 0.055	n.d.	0.028 ± 0.007	0.078 ± 0.026	0.074 ± 0.011	0.215 ± 0.022
Sm	μgL^{-1}	0.007 ± 0.005	0.012 ± 0.011	0.018 ± 0.017	n.d.	0.011 ± 0.005	0.019 ± 0.007	0.018 ± 0.006	0.063 ± 0.005
Eu	μgL^{-1}	0.013 ± 0.012	0.019 ± 0.018	0.036 ± 0.034	n.d.	0.022 ± 0.018	0.014 ± 0.005	0.035 ± 0.032	0.142 ± 0.052
Gd	μgL^{-1}	0.009 ± 0.006	0.013 ± 0.011	0.019 ± 0.017	n.d.	0.015 ± 0.003	0.019 ± 0.007	0.021 ± 0.005	0.068 ± 0.008
Dy	μgL^{-1}	0.011 ± 0.009	0.012 ± 0.009	0.016 ± 0.015	n.d.	0.023 ± 0.004	0.019 ± 0.005	0.02 ± 0.005	0.061 ± 0.012
Ho	μgL^{-1}	0.002 ± 0.001	0.003 ± 0.002	0.005 ± 0.004	n.d.	n.d.	0.004 ± 0.002	0.004 ± 0.0008	0.018 ± 0.004
Er	μgL^{-1}	0.015 ± 0.013	0.006 ± 0.005	0.01 ± 0.009	n.d.	0.029 ± 0.002	0.012 ± 0.003	0.013 ± 0.002	0.041 ± 0.008
Tm	μgL^{-1}	0.002 ± 0.001	0.002 ± 0.001	0.002 ± 0.001	n.d.	n.d.	0.002 ± 0.001	0.002 ± 0.0009	0.009 ± 0.001
Yb	μgL^{-1}	0.011 ± 0.009	0.006 ± 0.005	0.007 ± 0.005	n.d.	0.021 ± 0.003	0.01 ± 0.003	0.013 ± 0.004	0.04 ± 0.007
Lu	μgL^{-1}	0.002 ± 0.001	0.002 ± 0.001	0.002 ± 0.001	n.d.	n.d.	0.002 ± 0.001	0.002 ± 0.0006	0.01 ± 0.005
Hf	μgL^{-1}	0.0065 ± 0.0015	0.007 ± 0.006	0.01 ± 0.008	n.d.	0.0034 ± 0.0015	0.012 ± 0.003	0.012 ± 0.007	0.034 ± 0.026
W	μgL^{-1}	0.016 ± 0.009	0.083 ± 0.081	0.115 ± 0.112	n.d.	0.018 ± 0.004	0.059 ± 0.046	0.068 ± 0.054	0.026 ± 0.019
Pb	μgL^{-1}	0.199 ± 0.165	0.266 ± 0.181	0.487 ± 0.394	n.d.	0.094 ± 0.057	0.184 ± 0.067	0.256 ± 0.094	0.985 ± 0.124
Th	μgL^{-1}	0.015 ± 0.048	0.011 ± 0.009	0.015 ± 0.01	n.d.	0.011 ± 0.007	0.023 ± 0.007	0.018 ± 0.009	0.026 ± 0.006
U	μgL^{-1}	0.003 ± 0.002	0.006 ± 0.005	0.009 ± 0.008	n.d.	n.d.	0.01 ± 0.005	0.008 ± 0.004	0.029 ± 0.01

BGD
12, 1975–2019, 2015

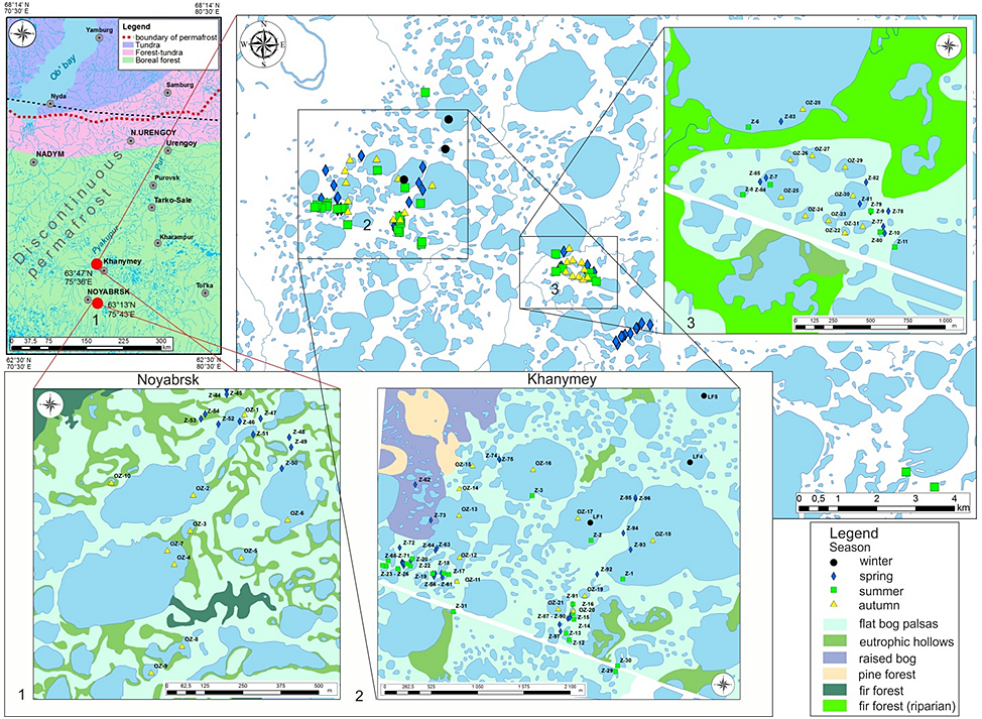

Figure 1. Study site area with symbols showing the position of sampled lakes and small water bodies in different seasons. Different colors correspond to different elementary ecosystems.

BGD
12, 1975–2019, 2015

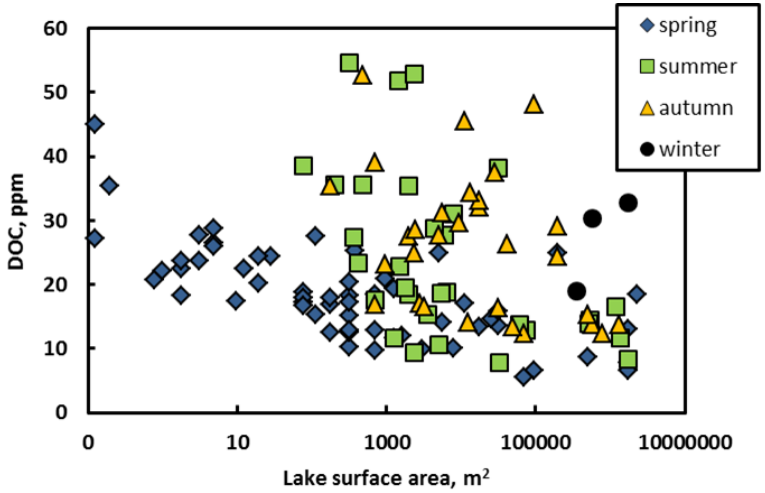

Figure 2. DOC concentration in thermokarst lakes of various sizes during four observation seasons.

BGD
12, 1975–2019, 2015

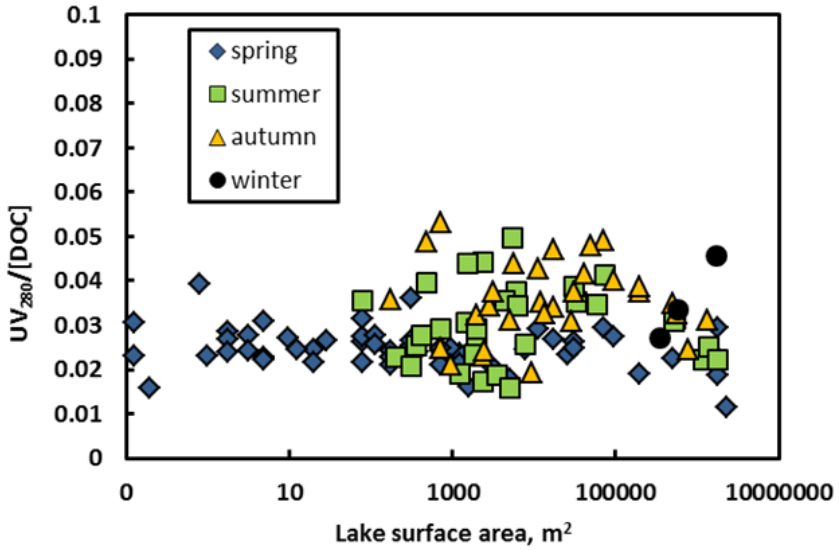

Figure 3. UV absorbance properties of thermokarst lake waters. The UV_{280}/DOC ratio increases in the order spring < summer < autumn ≤ winter, suggesting the progressive increase in aromaticity that is independent of the lake size.

BGD
12, 1975–2019, 2015

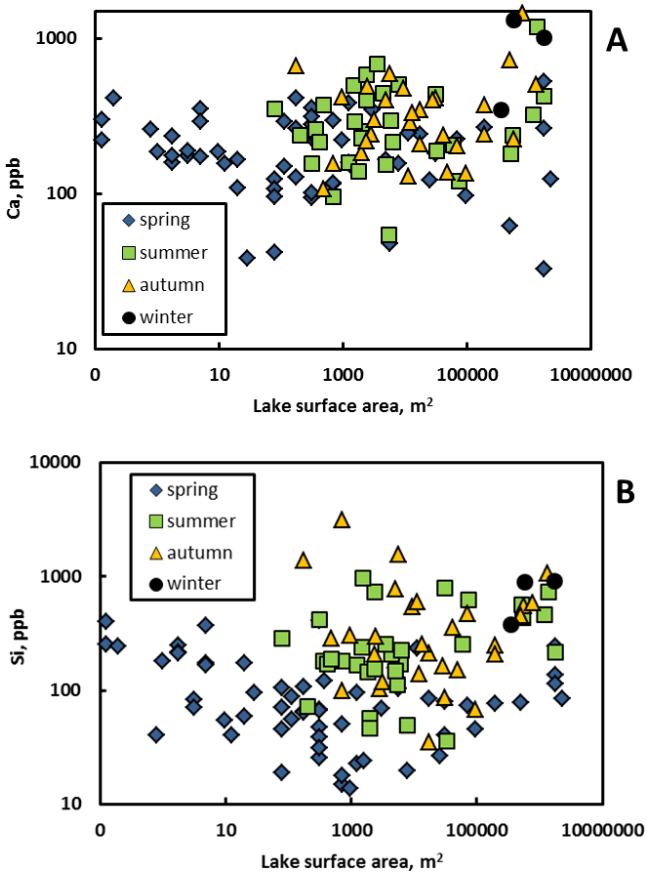

Figure 4. Significant variability, over 2 orders of magnitude, of Ca **(a)** and Si **(b)** concentrations in thermokarst lakes of a wide range of the lake area. Note the logarithmic scale in the element concentration.

BGD
12, 1975–2019, 2015

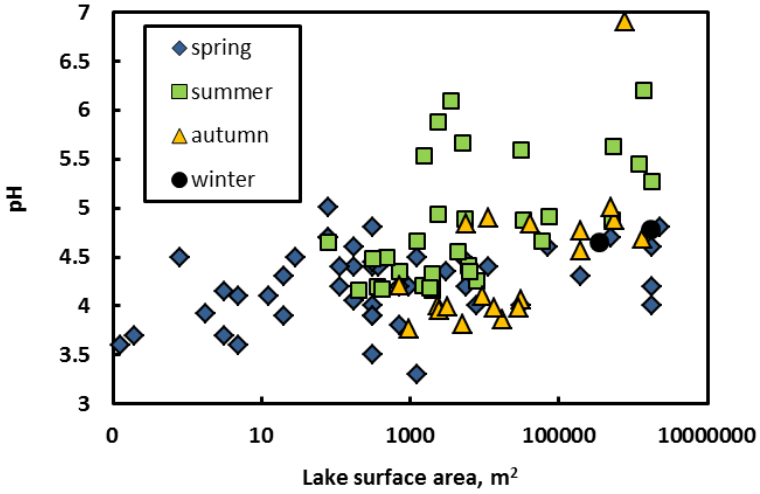

Figure 5. Increase in lake water pH with the increase in the lake size over four studied seasons. Note that the lowest pH is observed in spring and the highest in summer. This likely reflects the dominance of allochthonous organic input in the lake in spring, notably in the smallest water bodies, and autochthonous processes of some phytoplankton and macrophyte activity at the end of the summer.

BGD
12, 1975–2019, 2015

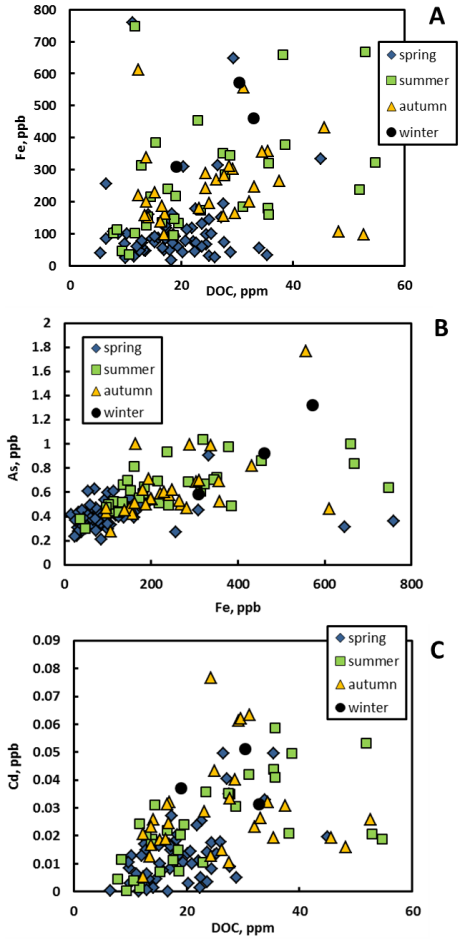

Figure 6. Examples of element concentrations in thermokarst lakes measured over different seasons; all lake sizes included.

BGD
12, 1975–2019, 2015

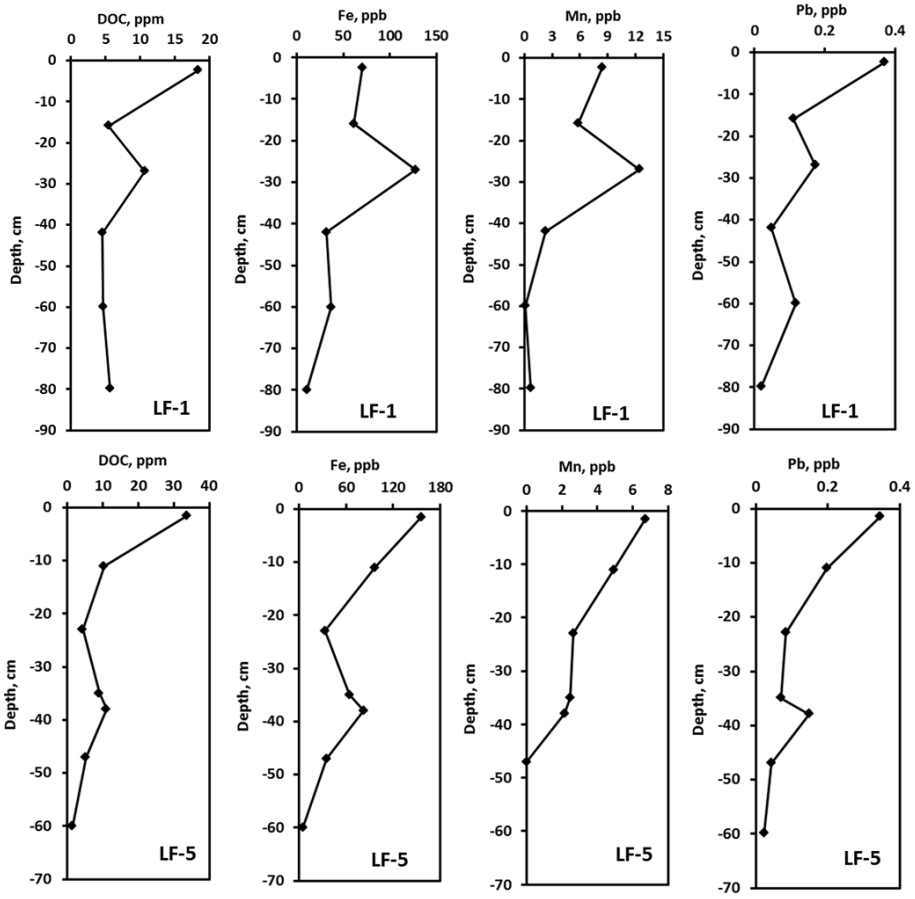

Figure 7. DOC, Fe, Mn and Pb concentrations in the ice cores of thermokarst lakes sampled in February 2014.

BGD
12, 1975–2019, 2015

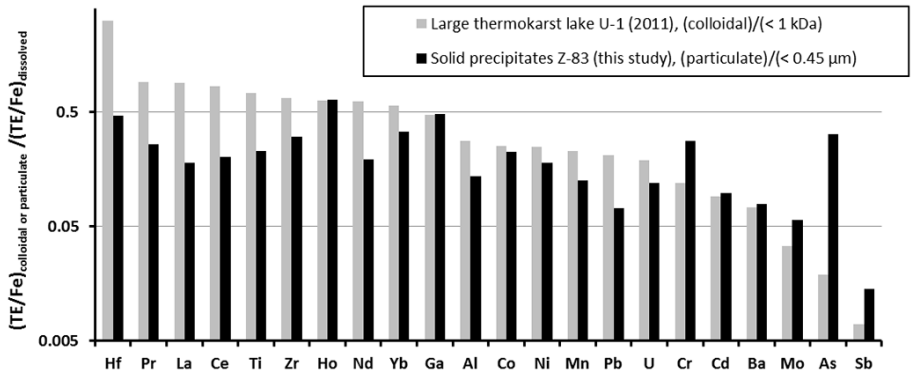

Figure 8. Comparison of the distribution coefficients of trace elements (TE) normalized to Fe between the solid precipitates collected in June from the ice surface of large lakes (Fig. S4) and filtered water (black columns) and those measured between colloids (1 kDa–0.45 µm) and the $LMW_{<1\,kDa}$ fraction in large thermokarst lakes (Pokrovsky et al., 2011) of discontinuous permafrost zones (grey columns).

BGD
12, 1975–2019, 2015

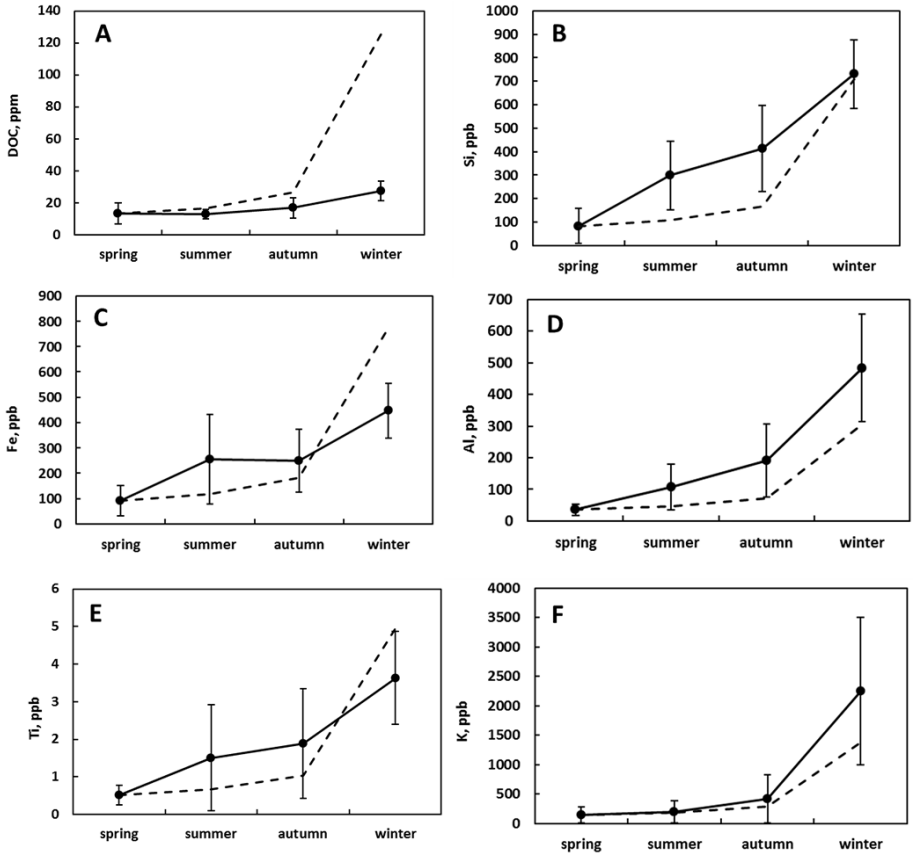

BGD
12, 1975–2019, 2015

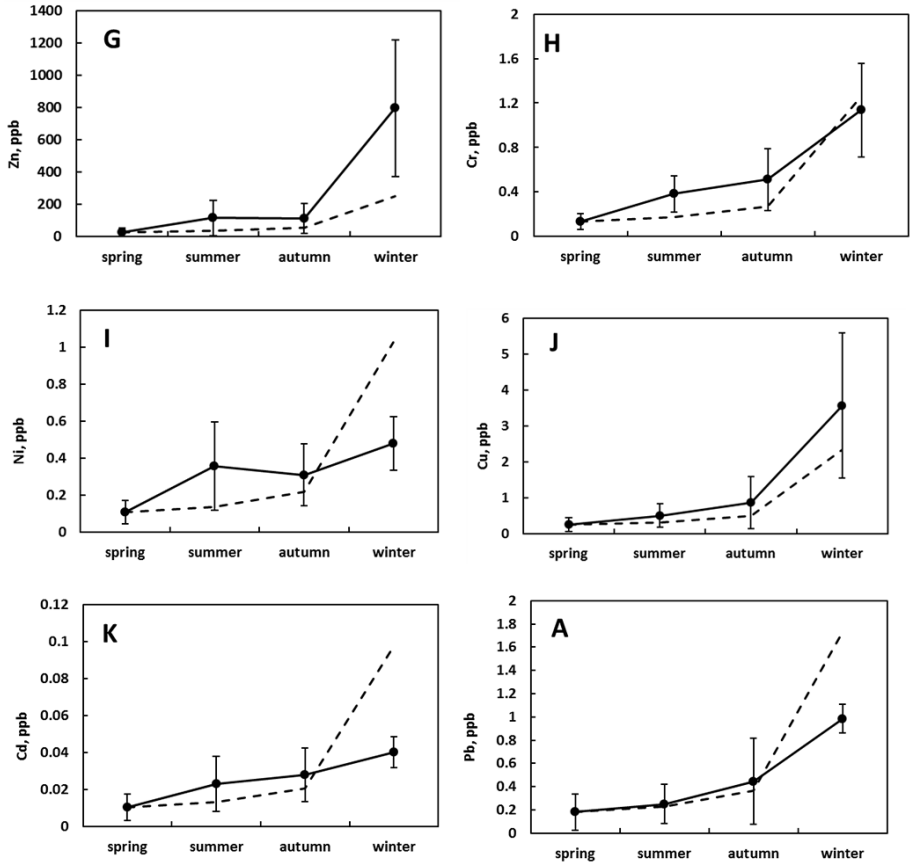

BGD
12, 1975–2019, 2015

Carbon and metals in thermokarst lakes

R. M. Manasypov et al.

Figure 9. Size-averaged concentrations of DOC **(a)**, Si **(b)**, Fe **(c)**, Al **(d)**, Ti **(e)**, and K **(f)** during different seasons. The points are the average and the error bars are the standard deviation. Only the medium and large lakes (> 100 m^2 surface area) were used for this estimation. The dotted line represents conservative behavior for a hypothetical lake of 75 cm depth in summer, 20 cm flooding in spring, 20 cm surface ice formation in October, and almost full freezing (10 cm bottom water left) in February. Zn **(g)**, Cr **(h)**, Ni **(i)**, Cu **(j)**, Cd **(k)** and Pb **(l)** average concentrations in thermokarst lakes during different seasons.

BGD
12, 1975–2019, 2015

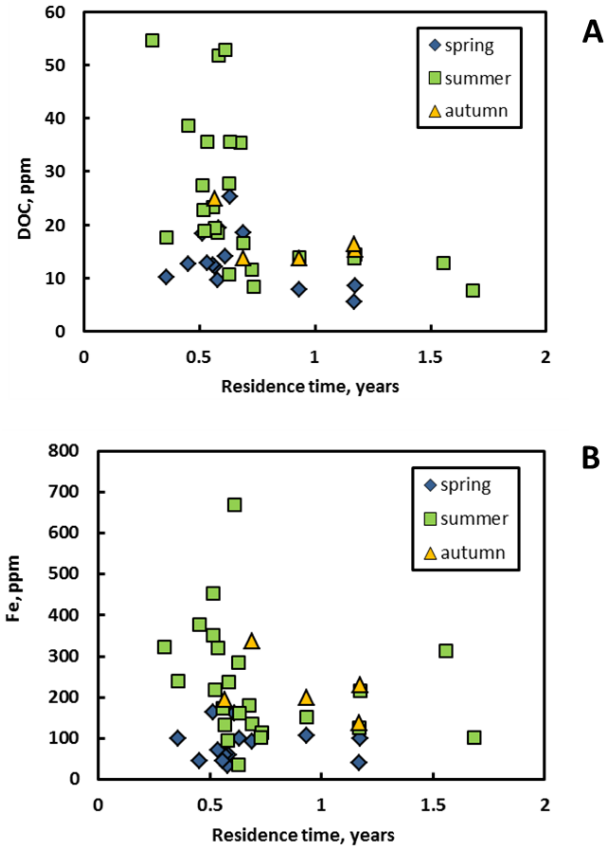

Figure 10. DOC **(a)** and Fe **(b)** concentrations during different seasons plotted as a function of water residence time in the water body.

BGD
12, 1975–2019, 2015

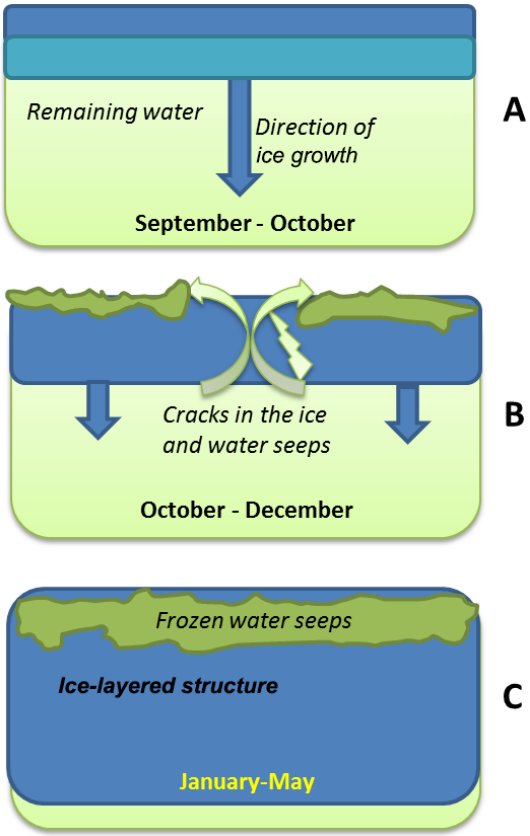

Figure 11. Sequence of ice crystallization events during the glacial period on the shallow (< 1 m depth) thermokarst lakes of western Siberia. **(a)** Start of the ice formation; **(b)** squeezing water towards the surface via seeps; **(c)** freezing of water pockets and seeps and multi-layer ice formation.

BGD
12, 1975–2019, 2015